Original Research
Date

Pseudo-Double Impulse for Simulating Critical Response of Elastic-Plastic MDOF Model under Near-Fault Earthquake Ground Motion

Hiroki Akehashi[1], Izuru Takewaki[1]*

[1]Department of Architecture and Architectural Engineering, Graduate School of Engineering, Kyoto University, Kyotodaigaku-Katsura, Nishikyo, Kyoto 615-8540, Japan

*** Correspondence:** Izuru Takewaki, Department of Architecture and Architectural Engineering, Graduate School of Engineering, Kyoto University, Kyotodaigaku-Katsura, Nishikyo, Kyoto 615-8540, Japan; E-mail takewaki@archi.kyoto-u.ac.jp

Abstract

A pseudo-double impulse (PDI) is proposed as an extension of the ordinary double impulse (DI) as a substitute of a one-cycle sine wave. PDI is treated as a set of impulsive lateral forces while the ordinary DI was introduced as an impulsive ground acceleration. The deformation and acceleration responses of multi-degree-of-freedom (MDOF) models under DI largely exceed those under the corresponding one-cycle sine wave as a main part of a near-fault ground motion. This is because DI has multiple frequency components and the higher-mode responses are excited. While the influence coefficient vector of the ordinary DI consists of 1 at every component, the influence coefficient vector of PDI is set to be proportional to the undamped fundamental natural mode. Therefore, the fundamental-mode response is mainly excited and the higher-mode responses are hardly excited by PDI. The displacement responses, the velocity responses and the input energy under DI and those under PDI are derived here for both elastic proportionally and non-proportionally damped MDOF models. The critical timing under PDI is also derived. The critical timing can be obtained by the time-history response analysis without repetition. It is demonstrated through the time-history response analysis that the distributions of interstory drifts and floor accelerations under the critical PDI correspond well to those under the critical one-cycle sine wave. Moreover, it is shown that, as far as the input level is large, the critical input period of PDI and that of the one-cycle sine wave correspond well. Since this procedure is not limited to elastic models, the proposed procedure helps to efficiently estimate the critical responses under the one-cycle sine wave for elastic-plastic MDOF models. Finally, the responses under recorded near-fault ground motions are compared with those under PDI. It is shown that the correspondence of the response under PDI and that under the recorded ground motions is fairly good although recorded ground motions are not always critical inputs for elastic-plastic MDOF models.

Keywords: Critical excitation, Elastic-plastic earthquake response, Nonlinear resonance, Double impulse, Pseudo-double impulse, Near-fault ground motion.

1. Introduction

Ground motions observed in recent years greatly exceed the level specified in the code for building structural design. Especially, a pulse-like motion and a long-period, long-duration motion could cause large damage to a specific class of building structures because these ground motions have characteristics extremely different from ground motions of random nature [1-3]. Therefore, it is necessary to establish a design method that takes account of the natures of these earthquake ground motions.

To develop effectively the seismic design against pulse-like motions, the following treatments may be necessary; 1) characterization and simplification of such ground motions and 2) investigation on the effectiveness of innovative base-isolation systems and structural control systems. Regarding the former, the expression of the pulse-like motions using trigonometric functions and wavelets have been investigated [4, 5]. It has also been clarified that a one-cycle sine wave effectively expresses a main characteristic of a fling-step motion [2, 6-8]. Since the relation among the parameters of the ground motion (e.g. the input frequency and the input amplitude), the structural parameters and the response quantities is quite complicated, an innovative approach has been desired. The critical excitation method using the worst input has been used to overcome this difficulty [9-12]. Regarding the latter, some researchers investigated the effectiveness of passive dampers under pulse-like motions [11-13]. It is also important to investigate the elastic-plastic response characteristics and the tendency of the structural damage under pulse-like motions [14-23].

The critical excitation method was initiated by Drenick [24] and has been investigated extensively [25, 26]. Kojima and Takewaki [27] introduced a simplified conceptual input called 'double impulse (DI)' as a substitute of the fling-step motion to capture the intrinsic natures of critical responses in closed form for elastic-plastic SDOF models. DI consists a set of two impulses, and its ground acceleration is defined by two parameters, V (velocity amplitude) and t_0 (time interval between two impulses). The most important subject on DI is to find the critical timing of two impulses under constant V. The closed-form solutions of the critical deformation responses and the critical timing for elastic-plastic SDOF models were derived based on the energy balance law. This critical excitation method using DI was applied to long-period, long-duration ground motions [9, 28].

As stated above, the transformation of ground motions into impulses enables one to derive the critical deformation for elastic-plastic SDOF models. On the other hand, for elastic-plastic MDOF models, only a few investigations have been conducted [29, 30]. In the case of MDOF models, the energy balance law cannot be used effectively due to the phase lag among masses, and floor acceleration responses under DI and those under the one-cycle sine wave do not correspond well due to the impulsive nature of DI [31]. In addition, the deformation responses of MDOF models with small damping under DI largely exceed those under the one-cycle sine wave. This is because DI has multiple frequency components different from the one-cycle sine wave. The overestimation of the responses may lead to extremely conservative designs. Moreover, the evaluation of floor acceleration responses is needed for the design of nonstructural components and facilities [32, 33].

In this paper, a pseudo-double impulse (PDI) is newly introduced. PDI is treated as a set of impulsive lateral forces while the ordinary DI was introduced as an impulsive ground acceleration. It is noted that the influence coefficient vector of PDI is set to be proportional to the undamped fundamental natural mode while the influence coefficient vector of the ordinary DI for a shear building model consists of 1 at every component. The fundamental-mode response is mainly excited and the higher-mode responses are hardly excited by PDI. The displacement responses, the velocity responses and the input energy under DI and those under PDI are derived here for both elastic proportionally and non-proportionally damped MDOF models. Finally, the time-history response analysis is conducted to compare the responses for elastic-plastic MDOF models under DI, PDI, the corresponding one-cycle sine wave, and recorded ground motions.

2. Response characteristics of elastic MDOF models under double impulse

It has been clarified that a one-cycle sine wave effectively expresses a main characteristic of a fling-step motion [2, 6-8]. Although the one-cycle sine wave is simple, the time-history response analysis is inevitable to obtain the maximum elastic-plastic response even for SDOF models. To respond to this issue, DI was introduced by Kojima and Takewaki [27] as a substitute of the fling-step motion. DI consists a set of two impulses, and its ground acceleration is defined by two parameters V (the velocity amplitude) and t_0 (the time interval between two impulses). This simple expression enables an independent treatment of the input period ($2t_0$) from the amplitude of the input. In addition, the closed-form solutions of the critical deformation responses and the corresponding critical time interval for elastic-plastic SDOF models can easily be derived based on the energy balance law. Moreover, the velocity amplitude V was adjusted so that the maximum value of the Fourier amplitude of DI coincides with that of the one-cycle sine wave. This treatment leads to a good correspondence of the Fourier amplitude of DI and that of the one-cycle sine wave in the range of $0 \le \omega \le 2\pi / t_0$. When t_0 is the critical time interval for the SDOF model, the transfer function of the SDOF model has the peak in this frequency range. Therefore, in the case of elastic-plastic SDOF models, DI works well as a substitute of the critical one-cycle sine wave.

In the case of elastic-plastic MDOF models, the contribution of higher modes to the responses under the one-cycle sine wave with relatively long period is slight. However, the higher modes are excited by DI because DI has multiple frequency components. This means that the use of DI may lead to the overestimation of the responses under the corresponding one-cycle sine wave. To overcome this difficulty, PDI is newly introduced in this paper. PDI is treated as a set of impulsive lateral forces. Especially, while the influence coefficient vector of the ordinary DI as an acceleration base input for a shear building model is the vector such that all the components are one, the influence coefficient vector of PDI is set to be proportional to the undamped fundamental natural mode. For elastic proportionally damped MDOF models, the response excited by PDI is equal to the fundamental mode response under DI. The ordinary DI introduced by Kojima and Takewaki represents a ground motion, and each impulse provides the change of the relative velocity response V to all the mass. On the other hands, the change of the relative velocity response along height provided by PDI is proportional to the undamped fundamental natural mode. It should be noted again that, PDI is a set of impulsive lateral forces, not a ground motion. Figure 1, 2 show the relation between DI, PDI and the corresponding one-cycle sine wave.

It should be noted that a one-cycle sine wave with short period may excite the higher-mode responses. In such case, the use of PDI is inappropriate since it mainly excites the fundamental natural mode response. However, a one-cycle sine wave with relatively long period, which mainly excites the fundamental natural mode response, often maximizes the deformation response of elastic-plastic MDOF models. Therefore, the response under PDI and that under the one-cycle sine wave correspond well in the critical case.

In this section, the responses of elastic MDOF models under DI are derived for the comparison with the responses under PDI, which will be derived in Section 3.

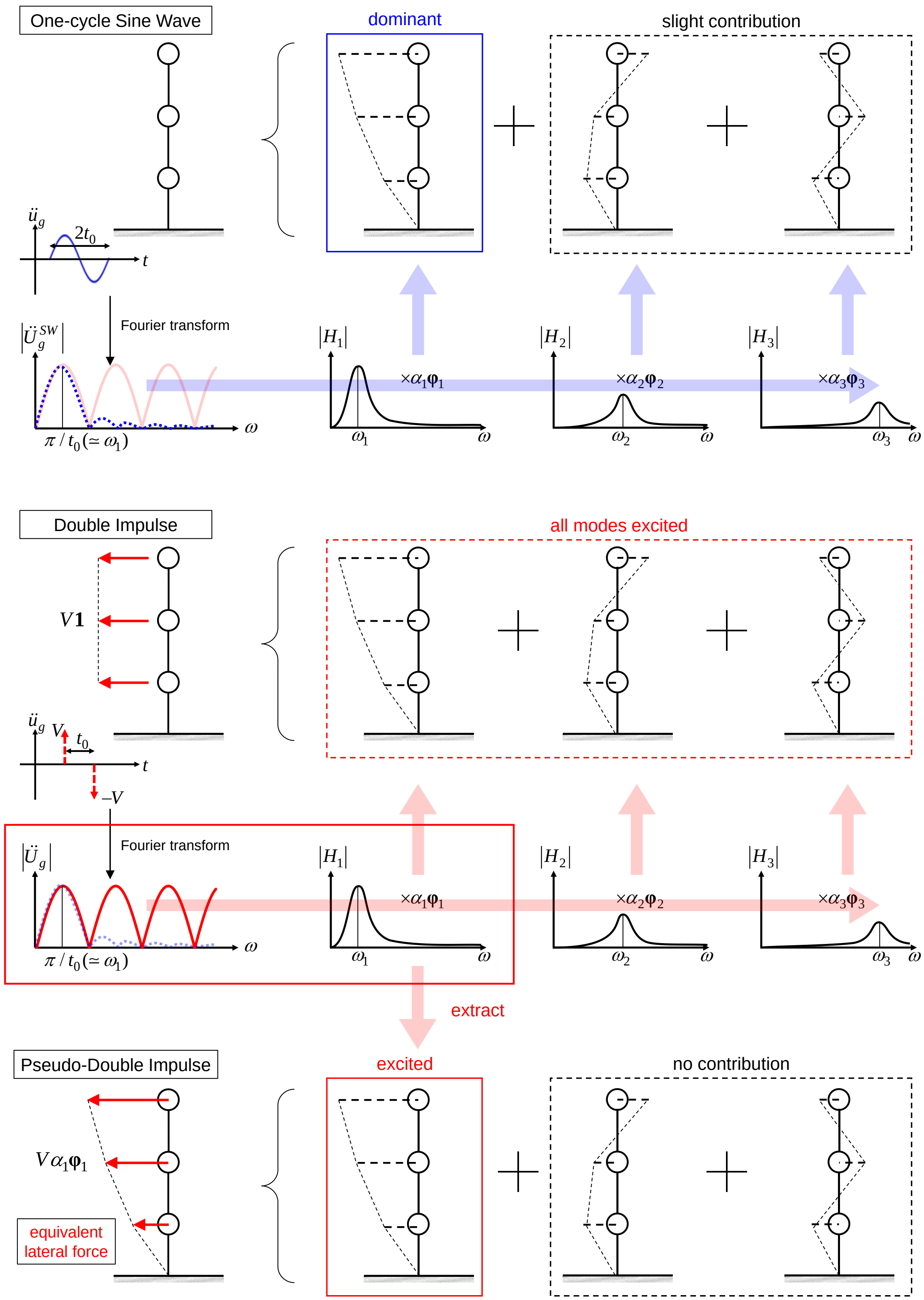

129

130 Figure 1 Comparison of modal responses under double impulse, pseudo-double impulse and one-
131 cycle sine wave

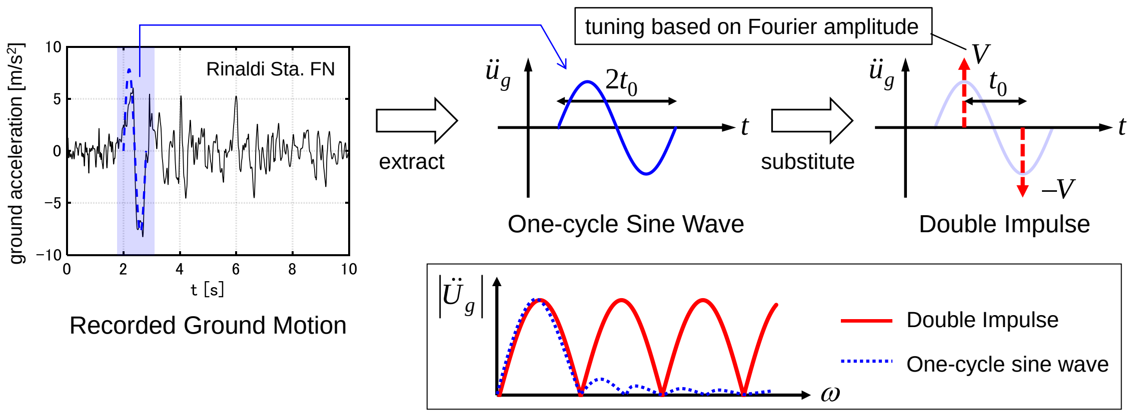

Figure 2 Relation between pulse-like ground motion, one-cycle sine wave and double impulse

2.1 Displacement response and input energy for elastic SDOF models under DI

Consider an SDOF model of mass m, undamped natural circular frequency ω_1, damping ratio h_1, damped natural circular frequency $\omega_{D1} = \omega_1\sqrt{1-h_1^2}$. The ground acceleration of DI is expressed by

$$\ddot{u}_g(t) = V\delta(t) - V\delta(t-t_0) \qquad (1)$$

where V is the input velocity amplitude, t_0 is the time interval of two impulses and $\delta(t)$ is the Dirac delta function.

The displacement response of an elastic SDOF model under DI can be expressed as follows.

$$u(t) = \frac{-Ve^{-h_1\omega_1 t}}{\omega_{D1}}\sin\omega_{D1}t \qquad (0 < t < t_0) \quad (2a)$$

$$u(t) = \frac{-Ve^{-h_1\omega_1 t}}{\omega_{D1}}\sin\omega_{D1}t + \frac{Ve^{-h_1\omega_1(t-t_0)}}{\omega_{D1}}\sin\omega_{D1}(t-t_0) \qquad (t > t_0) \quad (2b)$$

Furthermore, the velocity response can be expressed by

$$\dot{u}(t) = \frac{-Ve^{-h_1\omega_1 t}}{\sqrt{1-h_1^2}}\cos(\omega_{D1}t + \phi_1) \qquad (0 < t < t_0) \quad (3a)$$

$$\dot{u}(t) = \frac{-Ve^{-h_1\omega_1 t}}{\sqrt{1-h_1^2}}\cos(\omega_{D1}t + \phi_1) + \frac{Ve^{-h_1\omega_1(t-t_0)}}{\sqrt{1-h_1^2}}\cos(\omega_{D1}(t-t_0) + \phi_1) \qquad (t > t_0) \quad (3b)$$

where

$$\phi_1 = \arctan(h_1 / \sqrt{1-h_1^2}) \qquad (3c)$$

Since the impulse input does not change the displacement at once (the strain energy does not change at once), the input energies E_1, E_2 by the first and second impulses can be derived by subtracting the kinetic energy just before one impulse input from that just after that impulse input.

$$E_1 = \frac{1}{2} m V^2 \tag{4a}$$

$$\begin{aligned} E_2 &= \frac{1}{2} m V^2 \left\{ 1 - \frac{e^{-h_1 \omega_1 t_0}}{\sqrt{1-h_1^2}} \cos(\omega_{D1} t_0 + \phi_1) \right\}^2 - \frac{1}{2} m V^2 \left\{ \frac{e^{-h_1 \omega_1 t_0}}{\sqrt{1-h_1^2}} \cos(\omega_{D1} t_0 + \phi_1) \right\}^2 \\ &= \frac{1}{2} m V^2 \left\{ 1 - \frac{2e^{-h_1 \omega_1 t_0}}{\sqrt{1-h_1^2}} \cos(\omega_{D1} t_0 + \phi_1) \right\} \end{aligned} \tag{4b}$$

It should be remarked that an input energy can be expressed as $-\int m \dot{u} \ddot{u}_g dt$ in general.

In the case of MDOF models, the following relation is helpful in deriving E_1, E_2 for MDOF models.

$$\int f(t) \delta(t)\, dt = \frac{1}{2} \{ f(0-) + f(0+) \} \tag{5}$$

2.2 Displacement response and input energy of elastic, proportionally damped MDOF model under DI

Consider an elastic, proportionally damped MDOF model of n-th undamped natural mode vector $\boldsymbol{\varphi}_n$, n-th damping ratio h_n, undamped n-th natural circular frequency ω_n, mass matrix $\mathbf{M}$ and damped n-th natural circular frequency $\omega_{Dn} = \omega_n \sqrt{1-h_n^2}$. The displacement response of this model under DI can be expressed by

$$\mathbf{u}(t) = -\sum_{i=1}^{N} \left(\frac{\boldsymbol{\varphi}_i^T \mathbf{M} \mathbf{1}}{\boldsymbol{\varphi}_i^T \mathbf{M} \boldsymbol{\varphi}_i} \boldsymbol{\varphi}_i \right) \frac{V}{\omega_{Di}} e^{-h_i \omega_i t} \sin \omega_{Di} t \qquad (0 < t < t_0) \tag{6a}$$

$$\mathbf{u}(t) = -\sum_{i=1}^{N} \left(\frac{\boldsymbol{\varphi}_i^T \mathbf{M} \mathbf{1}}{\boldsymbol{\varphi}_i^T \mathbf{M} \boldsymbol{\varphi}_i} \boldsymbol{\varphi}_i \right) \frac{V}{\omega_{Di}} \left\{ e^{-h_i \omega_i t} \sin \omega_{Di} t - e^{-h_i \omega_i (t-t_0)} \sin \omega_{Di} (t-t_0) \right\} \qquad (t > t_0) \tag{6b}$$

Following the modal orthogonality with respect to the mass matrix, the displacements can be obtained as follows.

$$\mathbf{u}(t) = \sum_{i=1}^{N} \frac{-V e^{-h_i \omega_i t}}{\omega_{Di}} (\alpha_i \boldsymbol{\varphi}_i) \sin \omega_{Di} t \qquad (0 < t < t_0) \tag{7a}$$

$$\mathbf{u}(t) = \sum_{i=1}^{N} \frac{-V e^{-h_i \omega_i t}}{\omega_{Di}} (\alpha_i \boldsymbol{\varphi}_i) \sin \omega_{Di} t + \sum_{i=1}^{N} \frac{V e^{-h_i \omega_i (t-t_0)}}{\omega_{Di}} (\alpha_i \boldsymbol{\varphi}_i) \sin \omega_{Di} (t-t_0) \quad (t > t_0) \tag{7b}$$

where

$$\mathbf{1} = \alpha_1 \boldsymbol{\varphi}_1 + \ldots + \alpha_N \boldsymbol{\varphi}_N \tag{8}$$

The velocity response can then be expressed by

$$\dot{\mathbf{u}}(t) = \sum_{i=1}^{N} \frac{-Ve^{-h_i \omega_i t}}{\sqrt{1-h_i^2}} (\alpha_i \boldsymbol{\varphi}_i) \cos(\omega_{Di} t + \phi_i) \qquad (0 < t < t_0) \tag{9a}$$

$$\begin{aligned}\dot{\mathbf{u}}(t) = &\sum_{i=1}^{N} \frac{-Ve^{-h_i \omega_i t}}{\sqrt{1-h_i^2}} (\alpha_i \boldsymbol{\varphi}_i) \cos(\omega_{Di} t + \phi_i) \\ &+ \sum_{i=1}^{N} \frac{Ve^{-h_i \omega_i (t-t_0)}}{\sqrt{1-h_i^2}} (\alpha_i \boldsymbol{\varphi}_i) \cos(\omega_{Di} (t-t_0) + \phi_i)\end{aligned} \qquad (t > t_0) \tag{9b}$$

where

$$\phi_i = \arctan(h_i / \sqrt{1-h_i^2}) \tag{10}$$

The input energies E_1, E_2 by the first and second impulses can be expressed by

$$E_1 = \frac{1}{2} \sum_{i=1}^{N} V^2 (\alpha_i \boldsymbol{\varphi}_i)^T \mathbf{M1} = \frac{1}{2} \sum_{i=1}^{N} V^2 (\alpha_i \boldsymbol{\varphi}_i)^T \mathbf{M} (\alpha_i \boldsymbol{\varphi}_i) = \frac{1}{2} \sum_{i=1}^{N} M_i V^2 \tag{11a}$$

$$E_2 = \frac{1}{2} \sum_{i=1}^{N} M_i V^2 \left\{ 1 - \frac{2e^{-h_i \omega_i t_0}}{\sqrt{1-h_i^2}} \cos(\omega_{Di} t_0 + \phi_i) \right\} \tag{11b}$$

where $M_n = (\alpha_n \boldsymbol{\varphi}_n)^T \mathbf{M} (\alpha_n \boldsymbol{\varphi}_n)$ is the *n*-th generalized mass.

2.3 Displacement response and input energy of elastic, non-proportionally damped MDOF model under DI

Consider next an elastic, non-proportionally damped MDOF model. The displacement response of this model under DI can be expressed by

$$\mathbf{u}(t) = \sum_{i=1}^{N} Ve^{-h_i^* \omega_i^* t} \{ \boldsymbol{\beta}_i^g \cos(\omega_{Di}^* t) - \boldsymbol{\gamma}_i^g \sin(\omega_{Di}^* t) \} \qquad (0 < t < t_0) \tag{12a}$$

$$\begin{aligned}\mathbf{u}(t) = &\sum_{i=1}^{N} Ve^{-h_i^* \omega_i^* t} \{ \boldsymbol{\beta}_i^g \cos(\omega_{Di}^* t) - \boldsymbol{\gamma}_i^g \sin(\omega_{Di}^* t) \} \\ &- \sum_{i=1}^{N} Ve^{-h_i^* \omega_i^* (t-t_0)} \{ \boldsymbol{\beta}_i^g \cos(\omega_{Di}^* (t-t_0)) - \boldsymbol{\gamma}_i^g \sin(\omega_{Di}^* (t-t_0)) \}\end{aligned} \qquad (t > t_0) \tag{12b}$$

where $\boldsymbol{\psi}_n, \lambda_n = -h_n^* \omega_n^* + i\omega_{Dn}^* = -h_n^* \omega_n^* + i\omega_n^* \sqrt{1-(h_n^*)^2}, h_n^*, \omega_n^*$ denote the n-th complex eigenvector, the n-th eigenvalue, the n-th damping ratio and the n-th pseudo-undamped natural circular frequency, and

$$\boldsymbol{\beta}_n^g + i\boldsymbol{\gamma}_n^g = \frac{-2\boldsymbol{\psi}_n^T \mathbf{M1}}{2\lambda_n \boldsymbol{\psi}_n^T \mathbf{M} \boldsymbol{\psi}_n + \boldsymbol{\psi}_n^T \mathbf{C} \boldsymbol{\psi}_n} \boldsymbol{\psi}_n \tag{13}$$

Introducing the linear combination of the undamped natural modes, $\boldsymbol{\beta}_n^g, \boldsymbol{\gamma}_n^g$ can then be expressed as

$$\boldsymbol{\beta}_n^g = \beta_{n,1}^g \alpha_1 \boldsymbol{\varphi}_1 + \ldots + \beta_{n,N}^g \alpha_N \boldsymbol{\varphi}_N \tag{14a}$$

$$\boldsymbol{\gamma}_n^g = \gamma_{n,1}^g \alpha_1 \boldsymbol{\varphi}_1 + \ldots + \gamma_{n,N}^g \alpha_N \boldsymbol{\varphi}_N \tag{14b}$$

Let us define $\mu_{n,j}^g, \theta_{n,j}^g$ as

$$\mu_{n,j}^g = \omega_{Dn}^* \sqrt{(\beta_{n,j}^g)^2 + (\gamma_{n,j}^g)^2} \tag{15a}$$

$$\theta_{n,j}^g = \arctan(\beta_{n,j}^g / \gamma_{n,j}^g) \tag{15b}$$

Equations (14a, b), (15a, b) lead to

$$\mathbf{u}(t) = \sum_{i=1}^N \frac{-Ve^{-h_i^* \omega_i^* t}}{\omega_{Di}^*} \sum_{j=1}^N \mu_{i,j}^g (\alpha_j \boldsymbol{\varphi}_j) \sin(\omega_{Di}^* t - \theta_{i,j}^g) \qquad (0 < t < t_0) \tag{16a}$$

$$\begin{aligned} \mathbf{u}(t) = {} & \sum_{i=1}^N \frac{-Ve^{-h_i^* \omega_i^* t}}{\omega_{Di}^*} \sum_{j=1}^N \mu_{i,j}^g (\alpha_j \boldsymbol{\varphi}_j) \sin(\omega_{Di}^* t - \theta_{i,j}^g) \\ & + \sum_{i=1}^N \frac{Ve^{-h_i^* \omega_i^* (t-t_0)}}{\omega_{Di}^*} \sum_{j=1}^N \mu_{i,j}^g (\alpha_j \boldsymbol{\varphi}_j) \sin(\omega_{Di}^* (t-t_0) - \theta_{i,j}^g) \end{aligned} \qquad (t > t_0) \tag{16b}$$

The parameter $\mu_{i,j}^g$ can be regarded as a weighting coefficient of the undamped j-th mode vector component in the i-th complex mode. It is true that $\mu_{i,j}^g$ is dominant among $\mu_{i,1}^g, \ldots, \mu_{i,N}^g$ as far as the damping matrix has weak non-proportionality.

The velocity response can be expressed by

$$\dot{\mathbf{u}}(t) = \sum_{i=1}^N \frac{-Ve^{-h_i^* \omega_i^* t}}{\sqrt{1-(h_i^*)^2}} \sum_{j=1}^N \mu_{i,j}^g (\alpha_j \boldsymbol{\varphi}_j) \cos(\omega_{Di}^* t - \theta_{i,j}^g + \phi_i^*) \quad (0 < t < t_0) \tag{17a}$$

$$\begin{aligned}\dot{\mathbf{u}}(t) &= \sum_{i=1}^{N} \frac{-Ve^{-h_i^* \omega_i^* t}}{\sqrt{1-(h_i^*)^2}} \sum_{j=1}^{N} \mu_{i,j}^g (\alpha_j \boldsymbol{\varphi}_j) \cos(\omega_{Di}^* t - \theta_{i,j}^g + \phi_i^*) \\ &+ \sum_{i=1}^{N} \frac{Ve^{-h_i^* \omega_i^* (t-t_0)}}{\sqrt{1-(h_i^*)^2}} \sum_{j=1}^{N} \mu_{i,j}^g (\alpha_j \boldsymbol{\varphi}_j) \cos(\omega_{Di}^* (t-t_0) - \theta_{i,j}^g + \phi_i^*) \end{aligned} \quad (t > t_0) \quad (17b)$$

where

$$\phi_i^* = \arctan(h_i^* / \sqrt{1-(h_i^*)^2}) \quad (18)$$

The input energies E_1, E_2 by the first and second impulses can be expressed by

$$E_1 = \frac{1}{2} \sum_{i=1}^{N} \frac{V^2}{\sqrt{1-(h_i^*)^2}} \sum_{j=1}^{N} \mu_{i,j}^g M_j \cos(-\theta_{i,j}^g + \phi_i^*) \quad (19a)$$

$$\begin{aligned} E_2 &= \frac{1}{2} \sum_{i=1}^{N} \frac{V^2}{\sqrt{1-(h_i^*)^2}} \sum_{j=1}^{N} \mu_{i,j}^g M_j \cos(-\theta_{i,j}^g + \phi_i^*) \\ &- \sum_{i=1}^{N} \frac{V^2 e^{-h_i^* \omega_i^* t_0}}{\sqrt{1-(h_i^*)^2}} \sum_{j=1}^{N} \mu_{i,j}^g M_j \cos(\omega_{Di}^* t_0 - \theta_{i,j}^g + \phi_i^*) \end{aligned} \quad (19b)$$

3. Concept of PDI and response characteristics of elastic MDOF models under PDI

In this section, PDI, which is a set of impulsive lateral forces, is introduced. The influence coefficient vector of PDI is set to be proportional to the undamped fundamental natural mode. The responses of elastic MDOF models under PDI are derived. It should be noted that. although the formulations for the responses of elastic MDOF models under PDI cannot be applied directly to the elastic-plastic MDOF models, the formulations for the critical input timings of PDI are applicable to elastic-plastic MDOF models. The critical input timings of PDI will be derived in Section 3.3. Moreover, additional investigations are presented in Appendices 1, 2 (transfer function of acceleration and phase properties of maximum responses).

3.1 Displacement response and input energy of elastic, proportionally damped MDOF model under PDI

When DI is treated as an equivalent lateral force, the equation of motion is expressed by

$$\mathbf{M}\ddot{\mathbf{u}} + \mathbf{C}\dot{\mathbf{u}} + \mathbf{K}\mathbf{u} = -\mathbf{M}\boldsymbol{\iota}(V\delta(t) - V\delta(t-t_0)) \quad (20)$$

where $\boldsymbol{\iota}, \mathbf{C}, \mathbf{K}$ denote the influence coefficient vector, the damping matrix and the stiffness matrix. In the case of the ground motion acceleration input as DI, $\boldsymbol{\iota}$ becomes $\mathbf{1}$ consisting of 1 at every component. The displacement response of an elastic, proportionally damped MDOF model under PDI can be expressed by

$$\mathbf{u}(t) = -\sum_{i=1}^{N} \left(\frac{\boldsymbol{\varphi}_i^T \mathbf{M} \boldsymbol{\iota}}{\boldsymbol{\varphi}_i^T \mathbf{M} \boldsymbol{\varphi}_i} \boldsymbol{\varphi}_i \right) \frac{V}{\omega_{Di}} e^{-h_i \omega_i t} \sin \omega_{Di} t \qquad (0 < t < t_0) \quad (21a)$$

$$\mathbf{u}(t) = -\sum_{i=1}^{N} \left(\frac{\boldsymbol{\varphi}_i^T \mathbf{M} \boldsymbol{\iota}}{\boldsymbol{\varphi}_i^T \mathbf{M} \boldsymbol{\varphi}_i} \boldsymbol{\varphi}_i \right) \frac{V}{\omega_{Di}} \left\{ e^{-h_i \omega_i t} \sin \omega_{Di} t - e^{-h_i \omega_i (t - t_0)} \sin \omega_{Di} (t - t_0) \right\} \quad (t > t_0) \quad (21b)$$

When $\boldsymbol{\iota} = \alpha_1 \boldsymbol{\varphi}_1$, this impulsive lateral force is called the pseudo-double impulse (PDI). The displacement response under PDI can be expressed by

$$\mathbf{u}(t) = \frac{-V e^{-h_1 \omega_1 t}}{\omega_{D1}} (\alpha_1 \boldsymbol{\varphi}_1) \sin \omega_{D1} t \qquad (0 < t < t_0) \quad (22a)$$

$$\mathbf{u}(t) = \frac{-V e^{-h_1 \omega_1 t}}{\omega_{D1}} (\alpha_1 \boldsymbol{\varphi}_1) \sin \omega_{D1} t + \frac{V e^{-h_1 \omega_1 (t - t_0)}}{\omega_{D1}} (\alpha_1 \boldsymbol{\varphi}_1) \sin \omega_{D1} (t - t_0) \quad (t > t_0) \quad (22b)$$

From Equations (7a, b), (22a, b), it is understood that the response excited by PDI is equal to the fundamental mode response under DI. The velocity response can be expressed by

$$\dot{\mathbf{u}}(t) = \frac{-V e^{-h_1 \omega_1 t}}{\sqrt{1 - h_1^2}} (\alpha_1 \boldsymbol{\varphi}_1) \cos(\omega_{D1} t + \phi_1) \qquad (0 < t < t_0) \quad (23a)$$

$$\begin{aligned} \dot{\mathbf{u}}(t) = & \frac{-V e^{-h_1 \omega_1 t}}{\sqrt{1 - h_1^2}} (\alpha_1 \boldsymbol{\varphi}_1) \cos(\omega_{D1} t + \phi_1) \\ & + \frac{V e^{-h_1 \omega_1 (t - t_0)}}{\sqrt{1 - h_1^2}} (\alpha_1 \boldsymbol{\varphi}_1) \cos(\omega_{D1} (t - t_0) + \phi_1) \end{aligned} \qquad (t > t_0) \quad (23b)$$

The input energy E_1, E_2 by the first and the second impulse of PDI can be expressed by

$$E_1 = \frac{1}{2} \sum_{i=1}^{N} V^2 (\alpha_i \boldsymbol{\varphi}_i)^T \mathbf{M} (\alpha_i \boldsymbol{\varphi}_i) = \frac{1}{2} M_1 V^2 \quad (24a)$$

$$E_2 = \frac{1}{2} M_1 V^2 \left\{ 1 - \frac{2 e^{-h_1 \omega_1 t_0}}{\sqrt{1 - h_1^2}} \cos(\omega_{D1} t_0 + \phi_1) \right\} \quad (24b)$$

3.2 Displacement response and input energy of elastic, non-proportionally damped MDOF model under PDI

The displacement response of an elastic, non-proportionally damped MDOF model under PDI can be expressed by

$$\mathbf{u}(t)=\sum_{i=1}^{N}Ve^{-h_i^*\omega_i^* t}\{\boldsymbol{\beta}_i\cos(\omega_{Di}^* t)-\boldsymbol{\gamma}_i\sin(\omega_{Di}^* t)\} \qquad (0<t<t_0) \qquad (25a)$$

$$\begin{aligned}\mathbf{u}(t)=&\sum_{i=1}^{N}Ve^{-h_i^*\omega_i^* t}\{\boldsymbol{\beta}_i\cos(\omega_{Di}^* t)-\boldsymbol{\gamma}_i\sin(\omega_{Di}^* t)\}\\&-\sum_{i=1}^{N}Ve^{-h_i^*\omega_i^*(t-t_0)}\{\boldsymbol{\beta}_i\cos(\omega_{Di}^*(t-t_0))-\boldsymbol{\gamma}_i\sin(\omega_{Di}^*(t-t_0))\}\end{aligned} \qquad (t>t_0) \qquad (25b)$$

where

$$\boldsymbol{\beta}_n+i\boldsymbol{\gamma}_n=\frac{-2\boldsymbol{\psi}_n^T\mathbf{M}(\alpha_1\boldsymbol{\varphi}_1)}{2\lambda_n\boldsymbol{\psi}_n^T\mathbf{M}\boldsymbol{\psi}_n+\boldsymbol{\psi}_n^T\mathbf{C}\boldsymbol{\psi}_n}\boldsymbol{\psi}_n \qquad (26)$$

Introducing the linear combination of the undamped natural modes as in Equations (14a, b), $\boldsymbol{\beta}_n,\boldsymbol{\gamma}_n$ can be expressed as

$$\boldsymbol{\beta}_n=\beta_{n,1}\alpha_1\boldsymbol{\varphi}_1+\ldots+\beta_{n,N}\alpha_N\boldsymbol{\varphi}_N \qquad (27a)$$

$$\boldsymbol{\gamma}_n=\gamma_{n,1}\alpha_1\boldsymbol{\varphi}_1+\ldots+\gamma_{n,N}\alpha_N\boldsymbol{\varphi}_N \qquad (27b)$$

Then, $\mu_{n,j},\theta_{n,j}$ are defined as

$$\mu_{n,j}=\omega_{Dn}^*\sqrt{(\beta_{n,j})^2+(\gamma_{n,j})^2} \qquad (28a)$$

$$\theta_{n,j}=\arctan(\beta_{n,j}/\gamma_{n,j}) \qquad (28b)$$

Equations (27a, b), (28a, b) lead to

$$\mathbf{u}(t)=\sum_{i=1}^{N}\frac{-Ve^{-h_i^*\omega_i^* t}}{\omega_{Di}^*}\sum_{j=1}^{N}\mu_{i,j}(\alpha_j\boldsymbol{\varphi}_j)\sin(\omega_{Di}^* t-\theta_{i,j}) \qquad (0<t<t_0) \qquad (29a)$$

$$\begin{aligned}\mathbf{u}(t)=&\sum_{i=1}^{N}\frac{-Ve^{-h_i^*\omega_i^* t}}{\omega_{Di}^*}\sum_{j=1}^{N}\mu_{i,j}(\alpha_j\boldsymbol{\varphi}_j)\sin(\omega_{Di}^* t-\theta_{i,j})\\&+\sum_{i=1}^{N}\frac{Ve^{-h_i^*\omega_i^*(t-t_0)}}{\omega_{Di}^*}\sum_{j=1}^{N}\mu_{i,j}(\alpha_j\boldsymbol{\varphi}_j)\sin(\omega_{Di}^*(t-t_0)-\theta_{i,j})\end{aligned} \qquad (t>t_0) \qquad (29b)$$

The velocity response can be expressed by

$$\dot{\mathbf{u}}(t)=\sum_{i=1}^{N}\frac{-Ve^{-h_i^*\omega_i^* t}}{\sqrt{1-(h_i^*)^2}}\sum_{j=1}^{N}\mu_{i,j}(\alpha_j\boldsymbol{\varphi}_j)\cos(\omega_{Di}^* t-\theta_{i,j}+\phi_i^*) \qquad (30a)$$

$$\dot{\mathbf{u}}(t)=\sum_{i=1}^{N}\frac{-Ve^{-h_i^*\omega_i^* t}}{\sqrt{1-(h_i^*)^2}}\sum_{j=1}^{N}\mu_{i,j}(\alpha_j\boldsymbol{\varphi}_j)\cos(\omega_{Di}^* t-\theta_{i,j}+\phi_i^*)$$
$$+\sum_{i=1}^{N}\frac{Ve^{-h_i^*\omega_i^*(t-t_0)}}{\sqrt{1-(h_i^*)^2}}\sum_{j=1}^{N}\mu_{i,j}(\alpha_j\boldsymbol{\varphi}_j)\cos(\omega_{Di}^*(t-t_0)-\theta_{i,j}+\phi_i^*) \tag{30b}$$

The input energies E_1, E_2 by the first and second impulses of PDI can be expressed by

$$E_1=\frac{1}{2}\sum_{i=1}^{N}\frac{V^2}{\sqrt{1-(h_i^*)^2}}\mu_{i,1}M_1\cos(-\theta_{i,1}+\phi_i^*) \tag{31a}$$

$$E_2=\frac{1}{2}\sum_{i=1}^{N}\frac{V^2}{\sqrt{1-(h_i^*)^2}}\mu_{i,1}M_1\cos(-\theta_{i,1}+\phi_i^*)$$
$$-\sum_{i=1}^{N}\frac{V^2e^{-h_i^*\omega_i^* t_0}}{\sqrt{1-(h_i^*)^2}}\mu_{i,1}M_1\cos(\omega_{Di}^* t_0-\theta_{i,1}+\phi_i^*) \tag{31b}$$

The parameter $\mu_{i,1}$ can be regarded as the weight of the undamped fundamental mode vector component in the *i*-th complex mode. Equations (31a, b) mean that the input energy to the *i*-th complex mode by PDI depends on only $\mu_{i,1}$, not on $\mu_{i,2},....,\mu_{i,N}$.

Unlike the case of proportionally damped MDOF models, all the complex modes for non-proportionally damped MDOF models are excited by PDI. However, the contribution of the higher modes is slight as far as the damping matrix has weak non-proportionality. In Section 4, the contribution of each mode will be investigated through the time-history response analysis.

3.3 Critical input timing of second impulse of PDI

Akehashi and Takewaki [10] derived the critical timing of the double impulse for MDOF models. In this section, the critical timing of PDI is derived.

The input energy E_2 by the second impulse of PDI can be expressed by

$$E_2=\frac{1}{2}(\dot{\mathbf{u}}+V\boldsymbol{\iota})^T\mathbf{M}(\dot{\mathbf{u}}+V\boldsymbol{\iota})-\frac{1}{2}\dot{\mathbf{u}}^T\mathbf{M}\dot{\mathbf{u}}=\dot{\mathbf{u}}^T\mathbf{M}(V\boldsymbol{\iota})+\frac{1}{2}V^2\boldsymbol{\iota}^T\mathbf{M}\boldsymbol{\iota} \tag{32}$$

where $\dot{\mathbf{u}}$ is the velocity just before the input of the second impulse. Introducing the linear combination of the undamped natural modes, $\dot{\mathbf{u}}$ and $\boldsymbol{\iota}$ can be expressed as

$$\dot{\mathbf{u}}=p_1(t_0)\alpha_1\boldsymbol{\varphi}_1+...+p_N(t_0)\alpha_N\boldsymbol{\varphi}_N \tag{33a}$$
$$\boldsymbol{\iota}=q_1\alpha_1\boldsymbol{\varphi}_1+...+q_N\alpha_N\boldsymbol{\varphi}_N \tag{33b}$$

Substituting Equations (33a, b) into Equation (32), another expression of E_2 is obtained as follows.

$$\begin{aligned} E_2 &= V(p_1(t_0)\alpha_1\boldsymbol{\varphi}_1 + ... + p_N(t_0)\alpha_N\boldsymbol{\varphi}_N)^T\mathbf{M}(q_1\alpha_1\boldsymbol{\varphi}_1 + ... + q_N\alpha_N\boldsymbol{\varphi}_N) + \frac{1}{2}V^2\boldsymbol{\iota}^T\mathbf{M}\boldsymbol{\iota} \\ &= V\{q_1M_1p_1(t_0) + ... + q_NM_Np_N(t_0)\} + \frac{1}{2}V^2\boldsymbol{\iota}^T\mathbf{M}\boldsymbol{\iota} \end{aligned} \tag{34}$$

The partial differentiation of E_2 with respect to t_0 provides

$$\frac{\partial E_2}{\partial t_0} = V\{q_1M_1\dot{p}_1(t_0) + ... + q_NM_N\dot{p}_N(t_0)\} \tag{35}$$

In the case of proportionally damped MDOF models, $M_n\dot{p}_n$ represents the *n*-th mode inertial force. Therefore, Equation (35) means that, when the weighted sum of the modal inertial forces attains zero, E_2 is maximized. In the case of non-proportionally damped MDOF models or the case of elastic-plastic MDOF models, Equation (35) is also applicable. However, Equation (35) does neither strictly provide the complex modal decomposition nor the elastic-plastic modal decomposition. For these models, Equation (35) means just a change of a reference coordinate system. It should be pointed out that $\dot{p}_n(t)$ is calculated by Equation (36), and the critical timing can be obtained by the time-history response analysis.

$$\boldsymbol{\varphi}_n^T\mathbf{M}\ddot{\mathbf{u}}(t) = \dot{p}_n(t)\alpha_n\boldsymbol{\varphi}_n^T\mathbf{M}\boldsymbol{\varphi}_n \quad \Rightarrow \quad \dot{p}_n(t) = \frac{\boldsymbol{\varphi}_n^T\mathbf{M}\ddot{\mathbf{u}}(t)}{\alpha_n\boldsymbol{\varphi}_n^T\mathbf{M}\boldsymbol{\varphi}_n} \tag{36}$$

It is also noted that, when $\boldsymbol{\iota}$ is equal to $\alpha_n\boldsymbol{\varphi}_n$, the critical timing for the elastic, proportionally damped MDOF models can be expressed by

$$\frac{\pi - 2\phi_n}{\omega_{Dn}} \tag{37}$$

4. Comparison of responses and input energy of elastic MDOF models under DI, PDI and one-cycle sine wave through time-history response analysis

In this section, the time-history response analysis is conducted to compare the responses of elastic MDOF models under DI, PDI, and the one-cycle sine wave. The input circular frequency ω_p and the velocity amplitude V_p of the one-cycle sine wave are set following [27], namely $\omega_p = \pi / t_0$, $V_p = 1.222V$. This adjustment gives a good correspondence of the Fourier amplitude of the one-cycle sine wave and that of DI in the range of $0 \le \omega \le 2\pi / t_0$ (see Figure 2). MATLAB has been used for the numerical analyses and all the codes have been originally made. The accuracy has been checked through the comparison with a general-purpose structural analysis software.

4.1 Models for numerical examples

Consider two shear building models of 12 stories with different damping distributions of passive dampers. Both models have a trapezoidal distribution of story stiffnesses ($k_1 / k_{12} = 4$). The undamped fundamental natural period is 1.2 [s]. All the floor masses have the same value. The common story height is 4 [m]. P-Model has stiffness proportional type damping and NP-Model has a uniform distribution of damping coefficients. For both models, the sum of damping coefficients is set to $10{\times}10^7$ [Ns/m]. The fundamental damping ratio of P-Model is 0.035. Figure 3 shows the 1-4th participation vectors (eigenmode $\times$ participation factor) and the undamped natural periods.

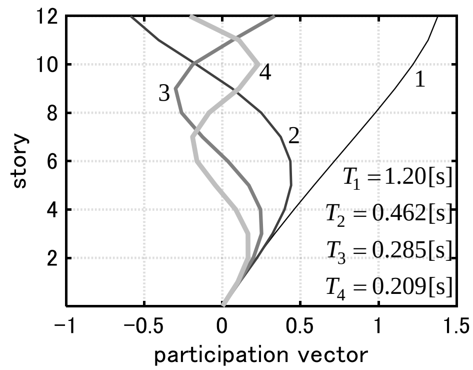

Figure 3 Participation vectors and natural periods

4.2 Comparison of elastic responses and input energy

Figures 4-9 show the distributions of peak interstory drifts, the distributions of floor accelerations, and the input energy under DI, PDI and the corresponding one-cycle sine wave for the inputs with $t_0 = 0.3, 0.6, 0.9$[s]. The time interval $t_0 = 0.6$[s] is nearly the critical timing for the fundamental natural mode. Figure 10 shows the time-history floor acceleration in the case of $t_0 = 0.6$[s]. The negative peak interstory drifts correspond to the maximum deformation after the first impulse, and the positive peak interstory drifts correspond to the maximum deformation after the second impulse. The velocity amplitude of DI is set to $V = 0.5$[m/s]. It can be observed from these figures that higher modes contribute to the responses under DI. This is because DI has multiple frequency components. It is also noted that, just after each impulse input, the change of the interstory velocity and the corresponding damping force are provided only in the first story, and the inertial force also arises to balance with the damping force. Therefore, the floor accelerations in lower stories becomes large. In the case of $t_0 = 0.6$[s], the responses under PDI and the one-cycle sine wave correspond well. The phase lag in the responses and the presence of the ground acceleration give the difference of the floor accelerations in lower stories. However, the difference is small. In the case of $t_0 = 0.9$[s], the higher-mode responses are hardly excited by both PDI and the one-cycle sine wave. However, the interstory drift response and the floor acceleration under PDI are about 1.3 times larger than those under the one-cycle sine wave. This results from the fact that DI has multiple frequency components and the input energy by PDI largely exceeds that by the one-cycle sine wave. In the case of $t_0 = 0.3[\mathrm{s}]$, the responses under PDI and the one-cycle sine wave do not correspond well. This is because the one-cycle sine wave excites not only the fundamental-mode response but also the second-mode response.

It can be observed from Figures 7-9 that the non-proportional damping provides the slight contribution of higher complex modes to the responses under PDI.

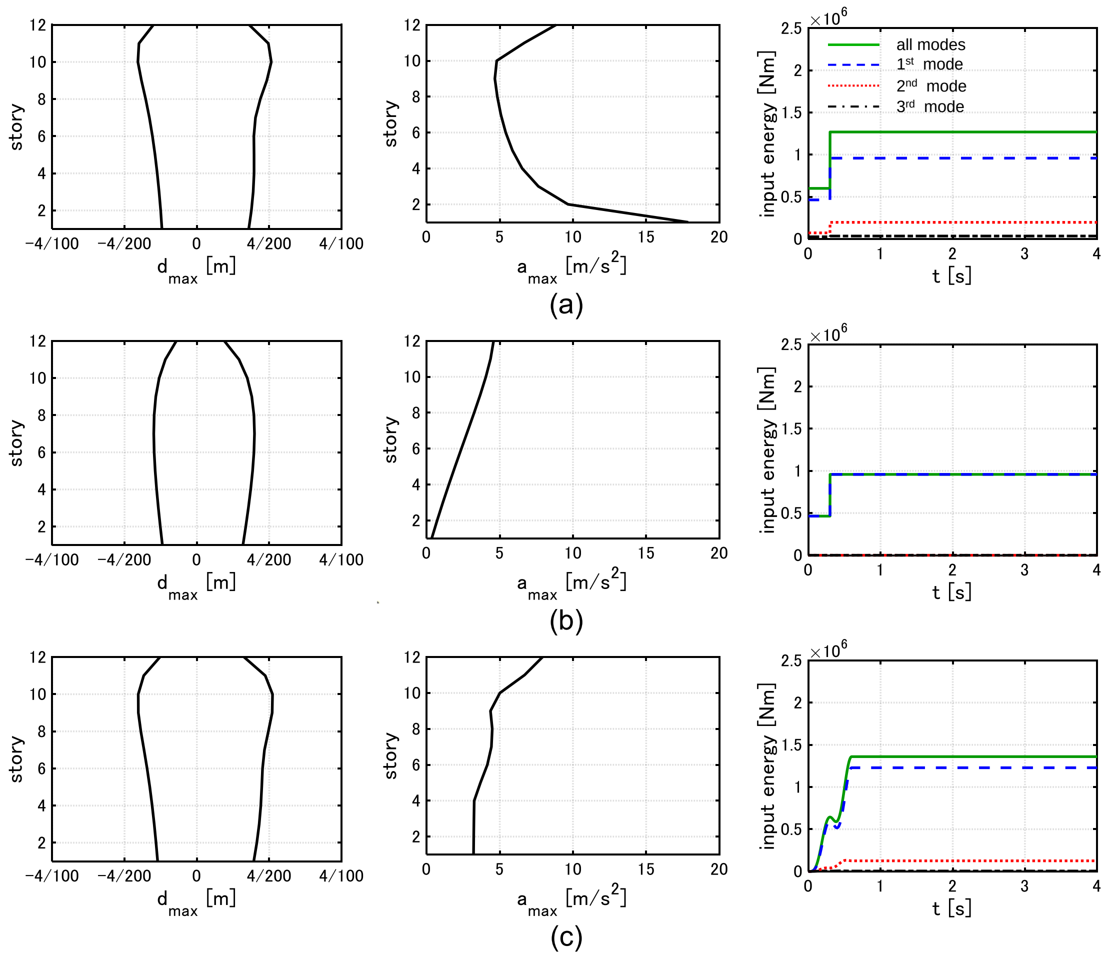

Figure 4 Comparison of distributions of interstory drifts, distributions of floor accelerations and input energy (P-Model, $t_0 = 0.3[\mathrm{s}]$), (a) DI, (b) PDI, (c) one-cycle sine wave.

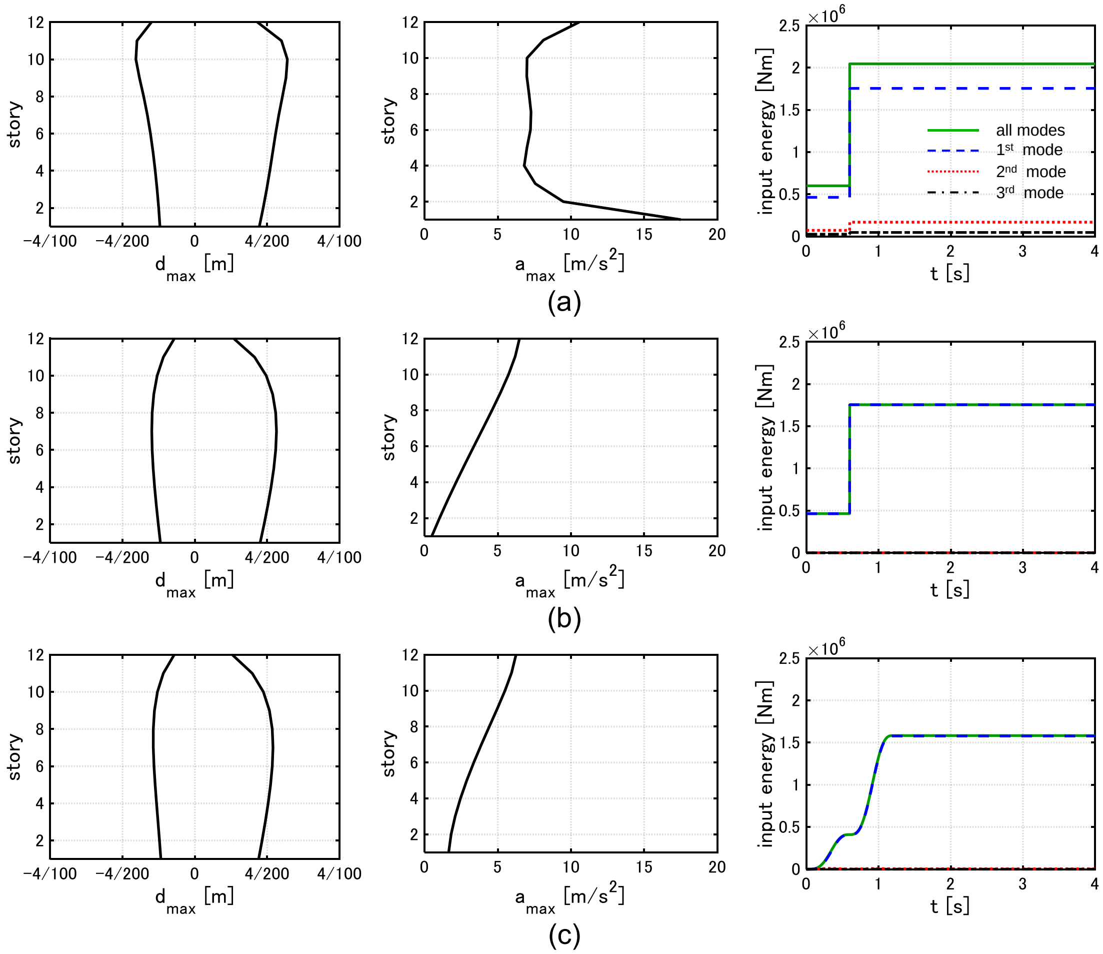

Figure 5 Comparison of distributions of interstory drifts, distributions of floor accelerations and input energy (P-Model, $t_0 = 0.6[\mathrm{s}]$), (a) DI, (b) PDI, (c) one-cycle sine wave.

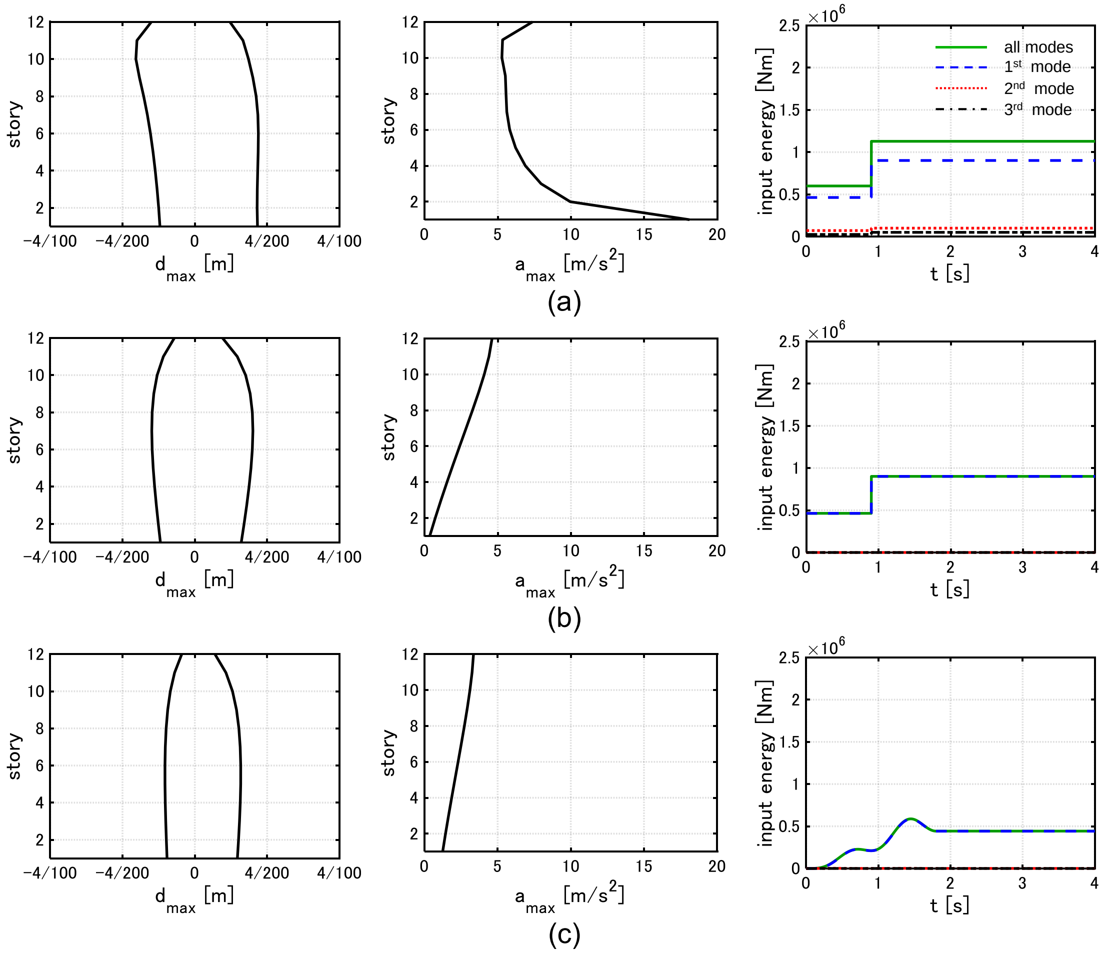

Figure 6 Comparison of distributions of interstory drifts, distributions of floor accelerations and input energy (P-Model, $t_0 = 0.9[\mathrm{s}]$), (a) DI, (b) PDI, (c) one-cycle sine wave.

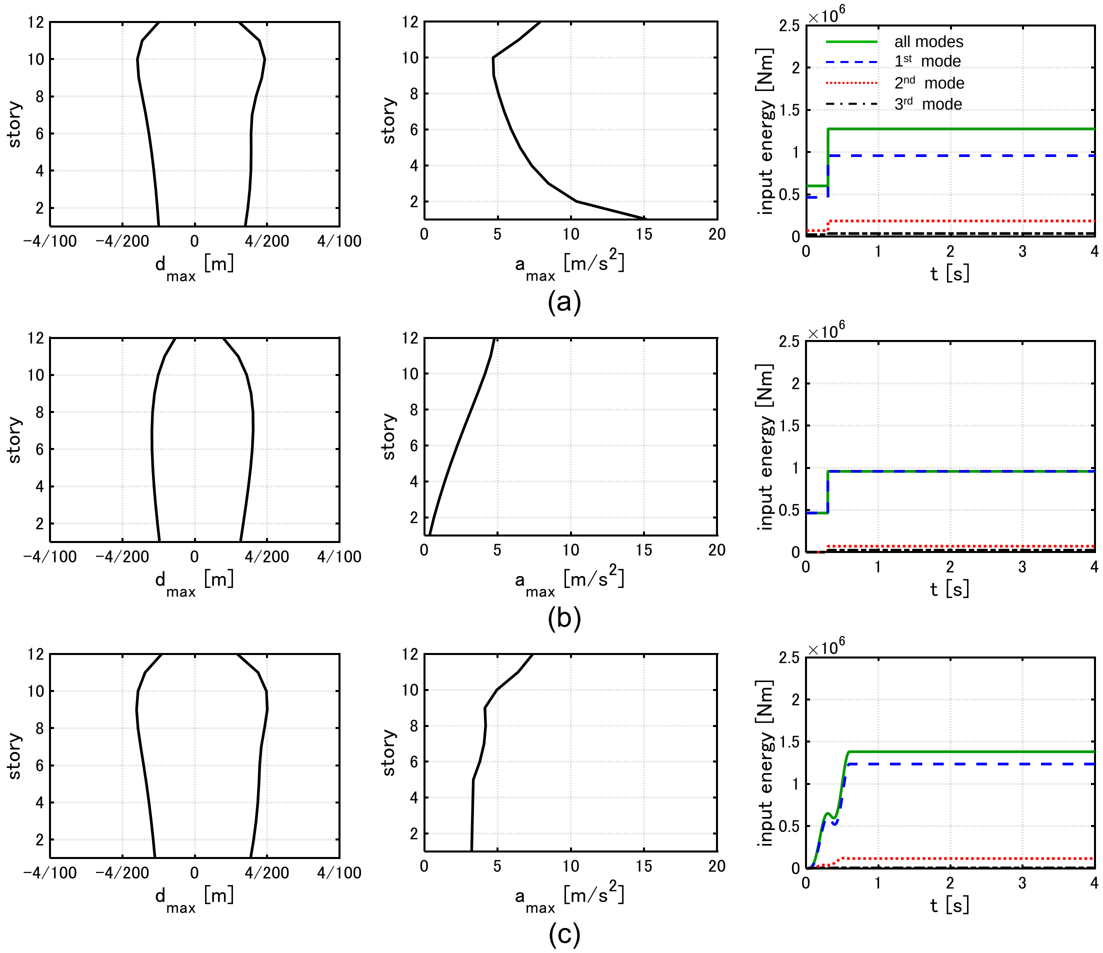

Figure 7 Comparison of distributions of interstory drifts, distributions of floor accelerations and input energy (NP-Model, $t_0 = 0.3$[s]), (a) DI, (b) PDI, (c) one-cycle sine wave.

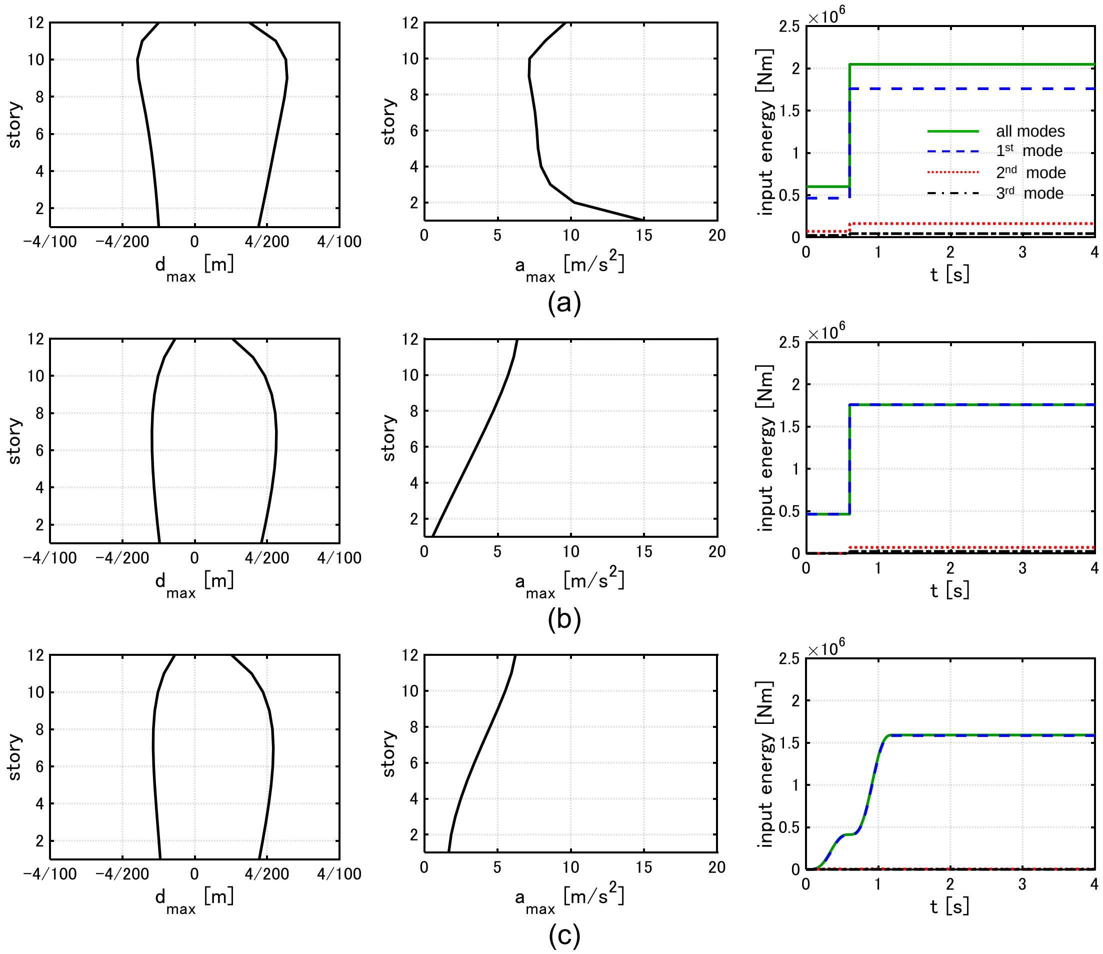

Figure 8 Comparison of distributions of interstory drifts, distributions of floor accelerations and input energy (NP-Model, $t_0 = 0.6[\mathrm{s}]$), (a) DI, (b) PDI, (c) one-cycle sine wave.

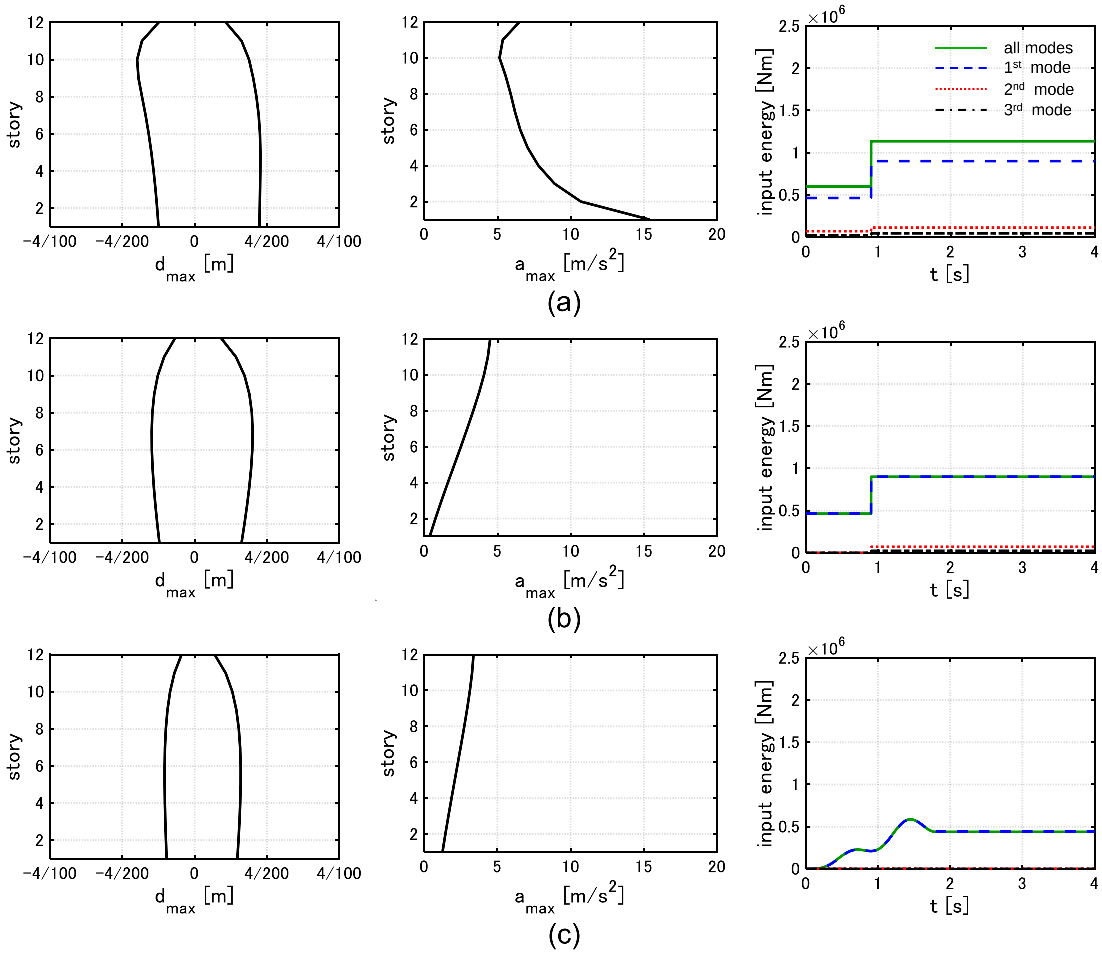

Figure 9 Comparison of distributions of interstory drifts, distributions of floor accelerations and input energy (NP-Model, $t_0 = 0.9$[s]), (a) DI, (b) PDI, (c) one-cycle sine wave.

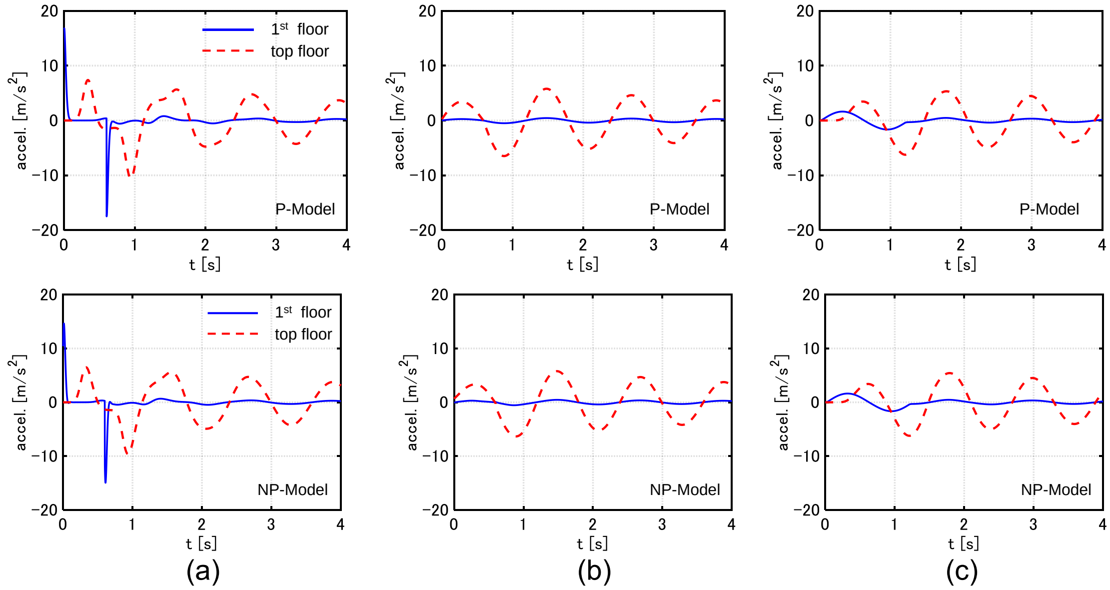

Figure 10 Time-history floor acceleration at 1st floor and top floor,
(a) DI ($t_0 = 0.6[\mathrm{s}]$), (b) PDI ($t_0 = 0.6[\mathrm{s}]$), (c) one-cycle sine wave ($t_0 = 0.6[\mathrm{s}]$).

Figure 11 shows the maximum interstory drift $d_{\max}$ with respect to t_0. The critical timing under DI and that under PDI are also illustrated. It can be observed that the critical timing under DI differs from the timing which maximizes the value of $d_{\max}$. On the other hand, the critical timing under PDI corresponds to the timing which maximizes the value of $d_{\max}$. Moreover, the value of $\max_{t_0}(d_{\max})$ under PDI is almost equal to that under the one-cycle sine wave.

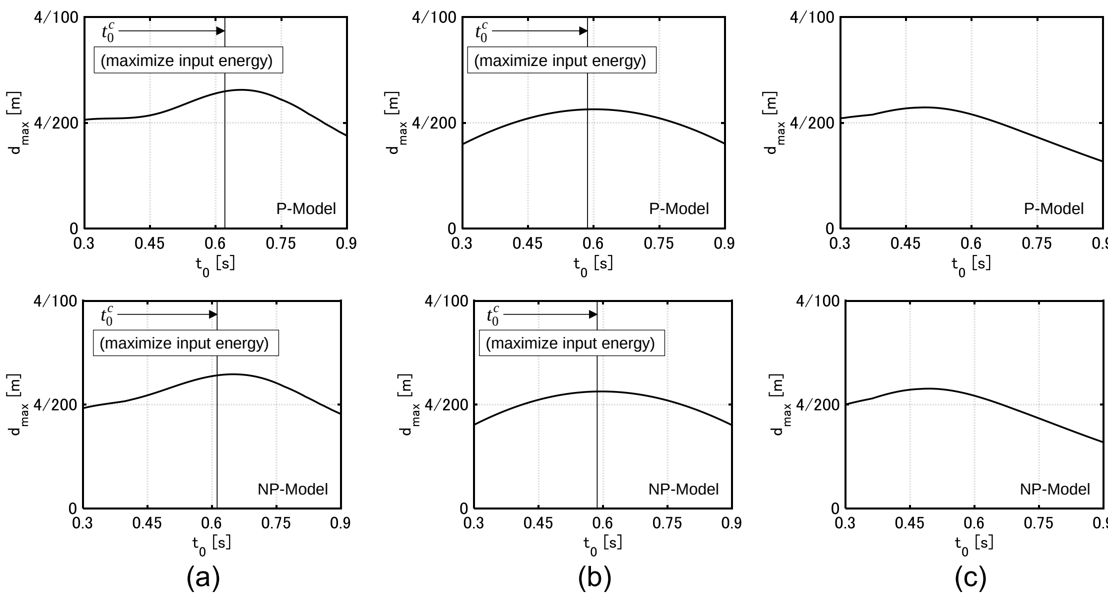

Figure 11 Maximum interstory drift with respect to t_0, (a) DI, (b) PDI, (c) one-cycle sine wave.

5. Comparison of responses and input energy of elastic-plastic MDOF models under DI, PDI and one-cycle sine wave through time-history response analysis

In this section, the time-history response analysis is conducted to compare the responses of elastic-plastic MDOF models under DI, PDI, and the one-cycle sine wave. P-Model and NP-Model are used again. The common yield interstory drift is 4/150 [m] and the story shear-interstory drift relation obeys the elastic perfectly-plastic rule. It should be pointed out that, due to the nonlinearity of the story restoring-force characteristics, the elastic modes and the plastic modes are coupled. The plastic modes mean the modes evaluated by using the post-yielding story stiffness. This phenomenon is called nonlinear coupling [34]. The contribution of the plastic modes to the responses depends on the state at the timing when the model attains the yield deformation. However, it is true that the fundamental mode is dominant in the response under PDI and that under the one-cycle sine wave with long period. Therefore, it is expected to investigate the correspondence of the elastic-plastic response under PDI and that under the one-cycle sine wave.

Figures 12-15 show the elastic-plastic responses under DI, PDI, and the one-cycle sine wave. Figure 12 indicates the input energy with respect to t_0. Figure 13 shows the maximum interstory drift with respect to t_0. In Figures 12, 13, the critical timing (maximizing the input energy) and the timing which maximizes the value of $d_{\max}$ at each input level are also plotted. Figures 14, 15 present the distributions of interstory drifts and the distributions of floor accelerations under the critical DI, and those under the critical PDI, and those under the one-cycle sine wave with t_0 which maximizes the value of $d_{\max}$ at each input level. The velocity level V is increased from $V = 0.5[\text{m/s}]$ to $V = 2.0[\text{m/s}]$ by 0.25 [m/s]. It can be observed from Figure 12 that t_0, which maximizes the input energy, smoothly shifts with the increase of the input level. Especially in the case of PDI, the critical timing and the timing which maximizes the value of $d_{\max}$ correspond well for all the input level. Moreover, the critical timing under PDI and the timing which maximizes the value of $d_{\max}$ under the one-cycle sine wave correspond well in the range of $V \geq 1.3[\text{m/s}]$. It can be observed from Figure 13 that, in the case of DI, $d_{\max}$ has multiple peaks with respect to t_0 under the condition of constant V. As a result, the timing which maximizes the value of $d_{\max}$ shows the unstable shift with the increase of the input level. In the case of PDI and the one-cycle sine wave, $d_{\max}$ has few peaks with respect to t_0 under the condition of constant V. Moreover, $\max_{t_0}(d_{\max})$ under PDI and that under the one-cycle sine wave correspond well for all input level. It can be observed from Figure 14 that the deformations in the middle stories under PDI are slightly larger than those under the one-cycle sine wave, and the deformations in the lower stories under PDI are slightly smaller than those under the one-cycle sine wave. However, the correspondence of the distributions of interstory drifts under PDI and those under the one-cycle sine wave is fairly good. On the other hand, the distributions of interstory drifts under DI do neither correspond to those under PDI nor those under the one-cycle sine wave. It can be observed from Figure 15 that the distributions of floor accelerations under PDI and those under the one-cycle sine wave correspond well. On the other hand, the floor acceleration response under DI is quite large.

From the above results, the distribution of interstory drifts and the distribution of floor accelerations under the critical PDI correspond well to those under the one-cycle sine wave with t_0 which maximizes the value of $d_{\max}$. As far as the input level is large, the critical timing under PDI corresponds well to the timing which maximizes the value of $d_{\max}$ under the one-cycle sine wave. Moreover, the critical timing can be obtained from the time-history response analysis without repetition. Therefore, using the critical PDI helps to efficiently estimate the responses and the input period under the critical one-cycle sine wave for elastic-plastic MDOF models.

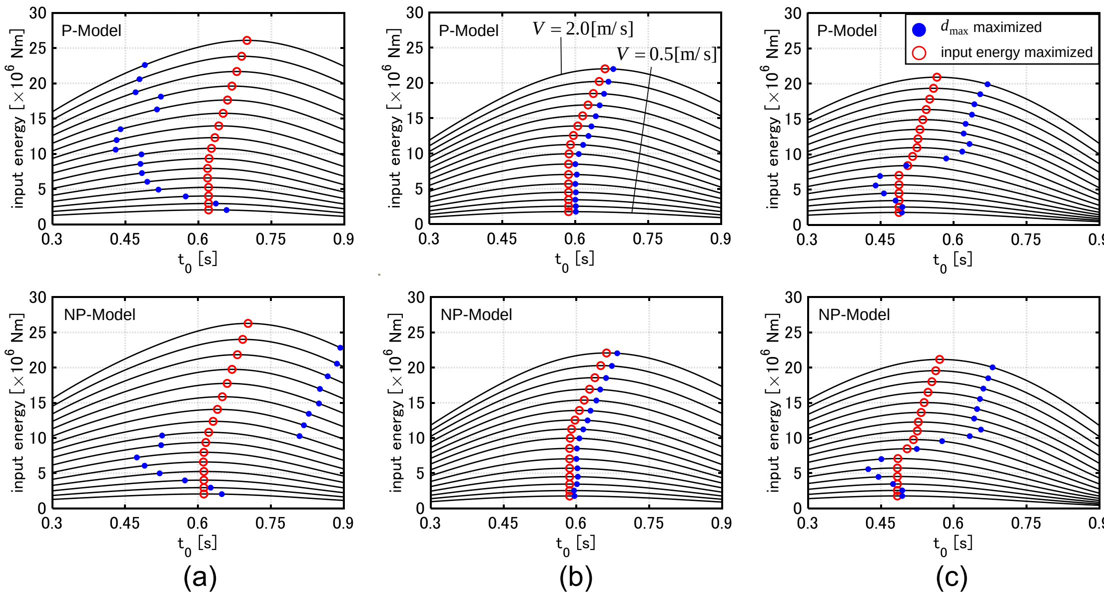

Figure 12 Input energy with respect to t_0, (a) DI, (b) PDI, (c) one-cycle sine wave.

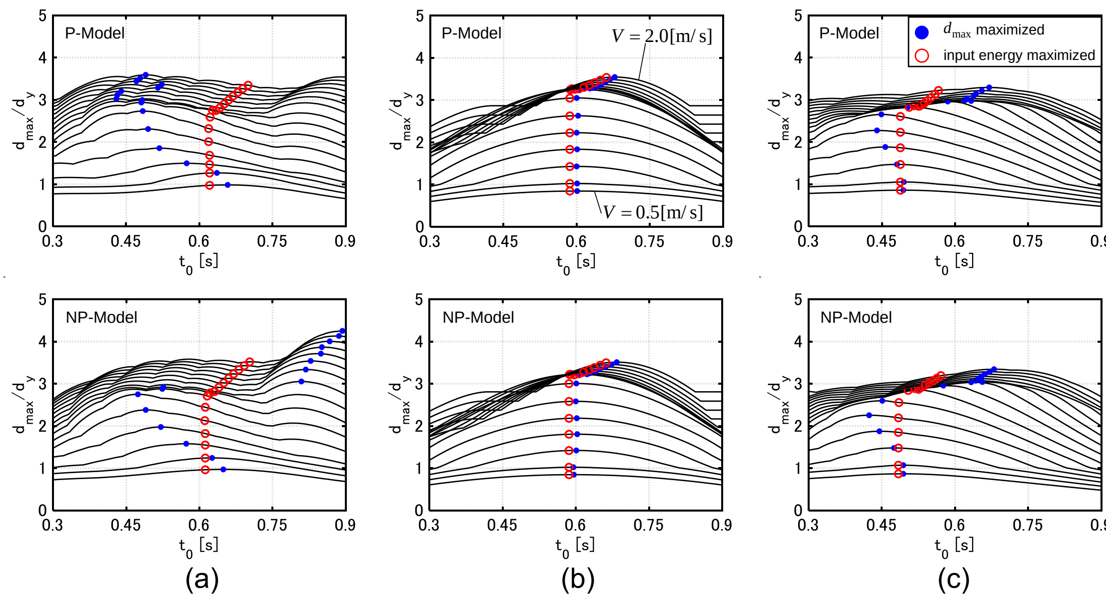

Figure 13 Maximum interstory drift with respect to t_0, (a) DI, (b) PDI, (c) one-cycle sine wave.

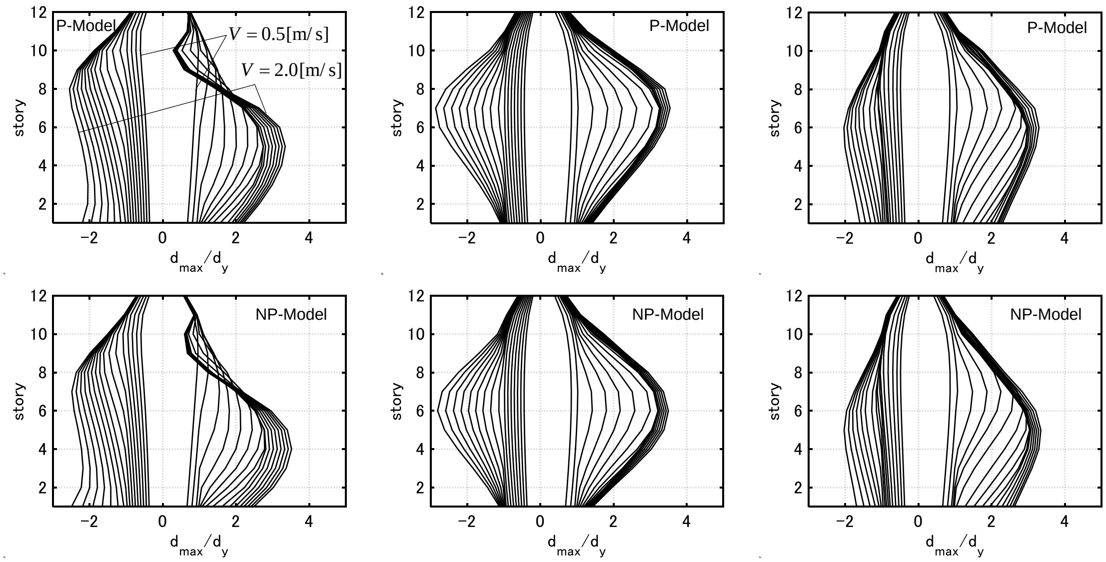

(a) (b) (c)

Figure 14 Distributions of interstory drifts, (a) critical DI, (b) critical PDI, (c) one-cycle sine wave with t_0 which maximizes value of $d_{\max}$ at each input level.

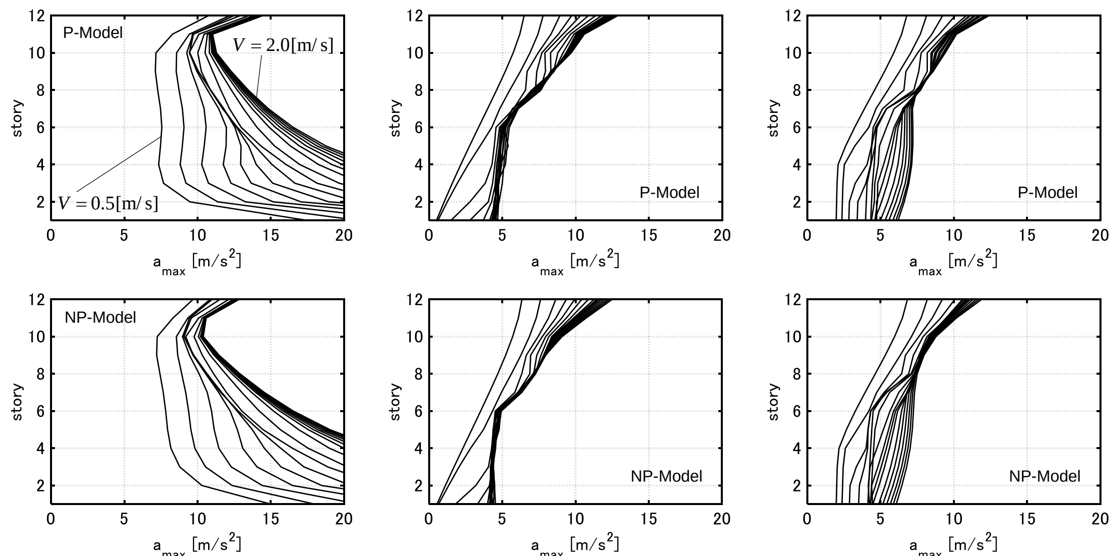

(a) (b) (c)

Figure 15 Distributions of floor accelerations, (a) critical DI, (b) critical PDI, (c) one-cycle sine wave with t_0 which maximizes value of $d_{\max}$ at each input level.

6. Comparison of responses of elastic-plastic MDOF models under recorded near-fault ground motions, DI, PDI and one-cycle sine wave through time-history response analysis

In this section, the time-history response analysis is conducted to compare the responses of elastic-plastic MDOF models under recorded near-fault ground motions, DI, PDI, and the corresponding one-cycle sine wave. In Sections 4, 5, the critical responses of the elastic-plastic MDOF models were mainly treated. However, recorded ground motions are not always critical inputs for the models. Therefore, the correspondence of the responses under PDI and those under recorded ground motions are investigated here. Application of the procedure presented in Section 5 (time modulation of PDI, i.e. time modulation of recorded ground motions for finding the critical input for a given structural model) will be discussed briefly at the end of this section.

The Rinaldi station fault-normal component during the Northridge earthquake in 1994 (Rinaldi Sta. FN) and the Kobe University NS component during the Hyogoken-Nanbu (Kobe) earthquake in 1995 (Kobe Univ. NS) are employed. The main part of each motion is approximated by a one-cycle sine wave following the procedure shown in [35]. Namely, the acceleration amplitude and the period of the approximated one-cycle sine wave for the Rinaldi station fault-normal component are $A_p = 7.85[\mathrm{m/s^2}], T_p = 0.8[\mathrm{s}]$ and those for the Kobe University NS component are $A_p = 2.6[\mathrm{m/s^2}], T_p = 1.0[\mathrm{s}]$. The time interval of impulses in DI and PDI is given by $T_p / 2$. The velocity amplitudes $V = 0.25, 1.0[\mathrm{m/s}]$ are selected for DI and PDI. The amplitudes of the ground motions and the approximated one-cycle sine waves are adjusted to the levels of DI and PDI. Under the velocity level $V = 0.25[\mathrm{m/s}]$, the models perform elastically. Figure 16 shows the adjusted ground accelerations of the recorded motions and the approximated one-cycle sine waves.

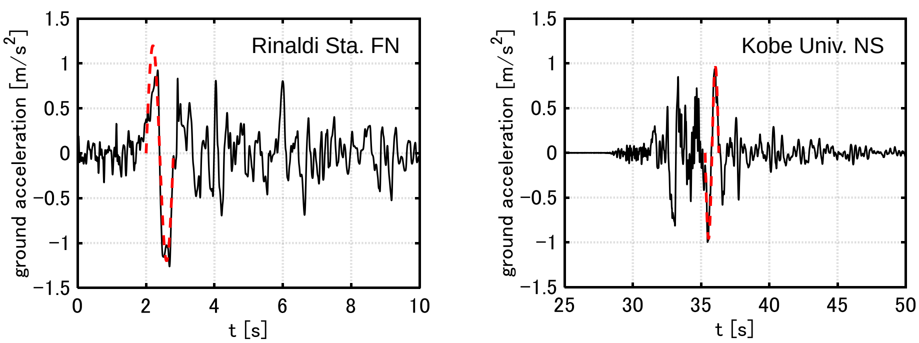

Figure 16 Accelerations of recorded ground motions and approximated one-cycle sine waves whose amplitudes are adjusted to the maximum velocity level $V = 0.25[\mathrm{m/s}]$ of DI and PDI, (a) Rinaldi Sta. FN, (b) Kobe Univ. NS

Figures 17 shows the elastic-plastic responses under Rinaldi Sta. FN, DI, PDI, and the approximated one-cycle sine waves for $V = 0.25, 1.0[\mathrm{m/s}]$. It can be observed that the distributions of interstory drifts and the distributions of floor accelerations under PDI slightly smaller than those under the ground motion and the one-cycle sine wave. This is because the time interval t_0 is shorter than the critical one. However, the correspondence of the distributions of interstory drifts under PDI and those under the ground motion and the one-cycle sine wave is fairly good. On the other hand, the distributions of floor accelerations under DI do not correspond to those under the ground motion, the one-cycle sine wave and PDI.

Figures 18 shows the elastic-plastic responses under Kobe Univ. NS, DI, PDI, and the approximated one-cycle sine wave. The distributions of interstory drifts and the distributions of floor accelerations under PDI and those under the one-cycle sine wave correspond well. On the other hand, the response under the ground motion is about 1.6-1.7 times larger than those under the one-cycle sine wave and PDI in the case of $V = 0.25[\mathrm{m/s}]$. This is because the ground acceleration of the Kobe University NS component becomes large at plural timings and the hysteretic energy dissipation does not exist in the elastic response range. In the case of $V = 1.0[\mathrm{m/s}]$, due to the residual deformation, the deformations in the lower stories under the ground motion slightly exceed those under PDI. However, the correspondence of the distributions of interstory drifts under the ground motion and PDI is fairly good. Moreover, the distributions of floor accelerations under PDI correspond well to those under the ground motion. As in the case of Rinaldi Sta. FN, the distributions of floor accelerations under DI do not correspond to those under the Kobe University NS component, the one-cycle sine wave and PDI.

From the above results, it can be concluded that the correspondence of the response under PDI and that under the recorded ground motions is fairly good although recorded ground motions are not always the critical inputs for elastic-plastic MDOF models. Especially, the floor acceleration response under PDI corresponds well to that under the ground motions while that under DI largely exceeds those.

Although the time modulation of recorded ground motions for finding the critical input for a given elastic-plastic MDOF model was not conducted, this procedure can be performed straightforwardly by using the procedure shown at the end of Section 5. If we do not use PDI, many repetitive procedures including time-history response analyses are necessary for the recorded ground motions to find the critically time-modulated version of recorded ground motions.

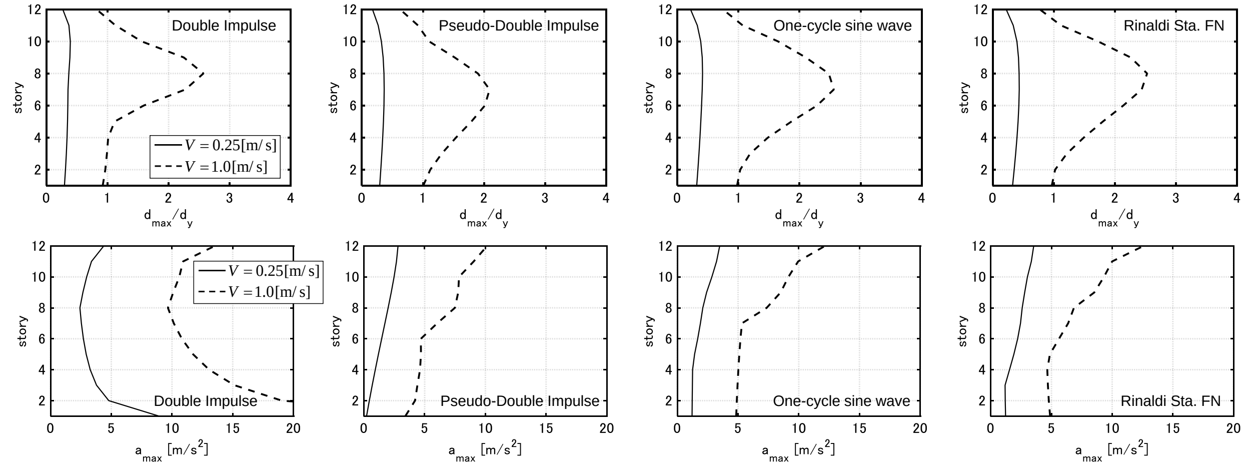

(a)

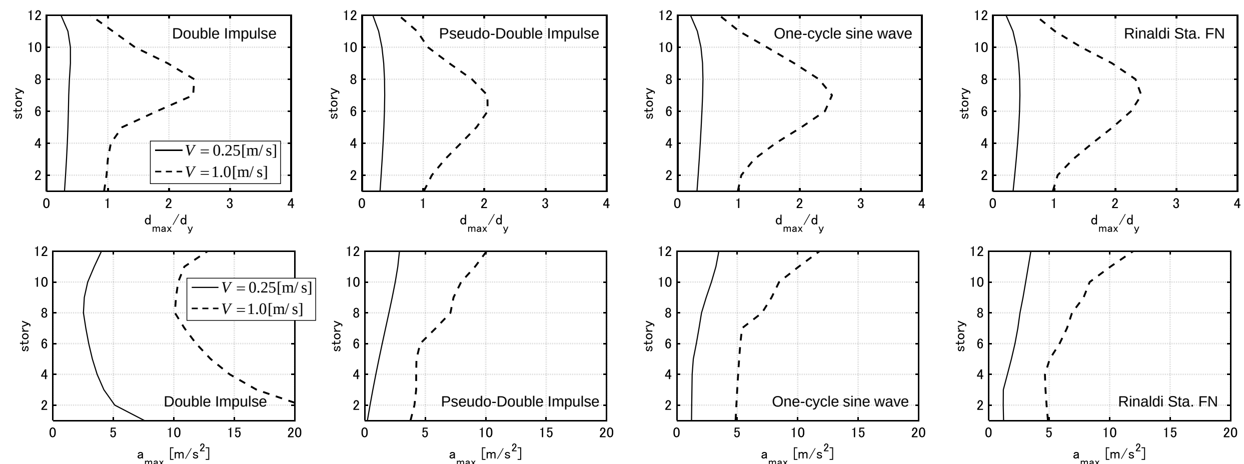

(b)

Figure 17 Distributions of interstory drifts and distributions of floor accelerations under Rinaldi Sta. FN, approximated one-cycle sine wave, DI and PDI, (a) P-Model, (b) NP-Model

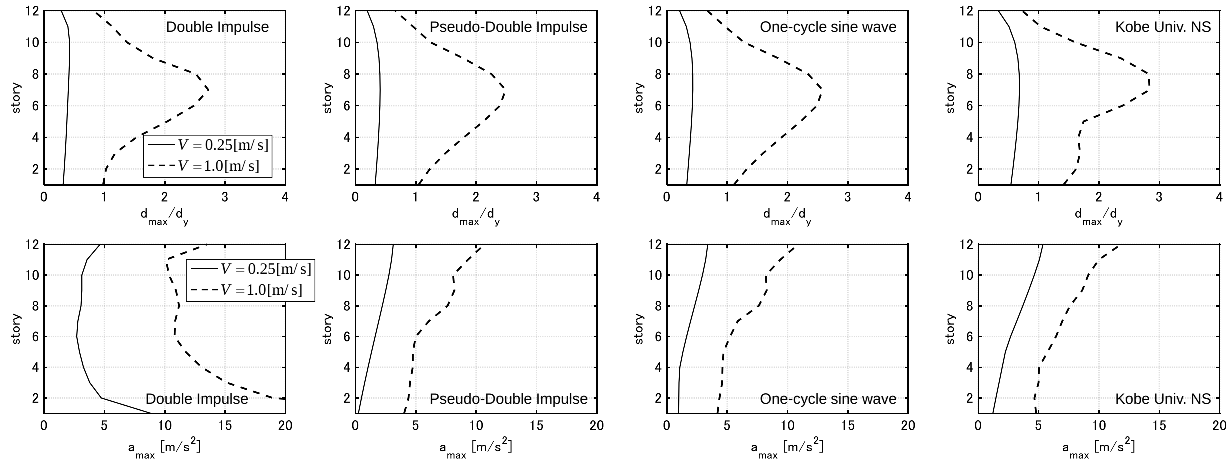

(a)

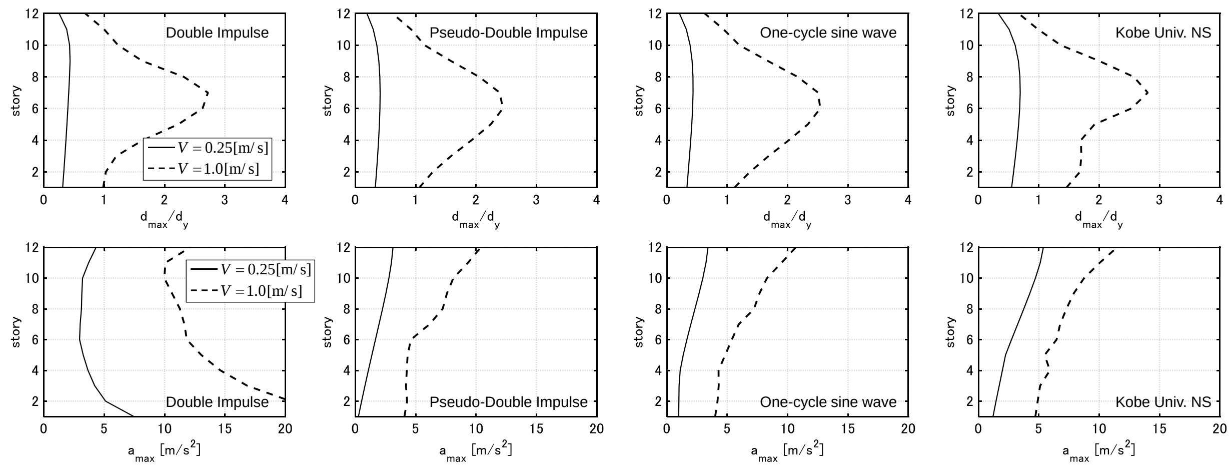

(b)

Figure 18 Distributions of interstory drifts and distributions of floor accelerations under Kobe Univ. NS, approximated one-cycle sine wave, DI and PDI, (a) P-Model, (b) NP-Model

7. Conclusions

In this paper, a pseudo-double impulse (PDI) was proposed as an extension of the ordinary double impulse (DI). The main conclusions can be summarized as follows.

(1) The deformation response and the acceleration response under DI largely exceed those under the corresponding one-cycle sine wave as a main part of a near-fault ground motion. This is because DI has multiple frequency components. To resolve this issue, PDI was introduced. PDI is treated as a set of impulsive lateral forces which is equivalent to an ordinary double impulse. While the influence coefficient vector of DI for a shear building model is the vector such that all the components are one, the influence coefficient vector of PDI is set to be proportional to the undamped fundamental natural mode.

(2) The displacement responses, the velocity responses and the input energy under DI and those under PDI were derived for both elastic proportionally damped MDOF models and elastic non-proportionally damped MDOF models. In the case of elastic proportionally damped MDOF models, the responses under PDI is equal to the fundamental mode response under DI. In the case of elastic non-proportionally damped MDOF models, all the complex modes are excited by PDI. However, the contribution of higher modes is slight as far as the non-proportionality of the damping matrix is small.

(3) The critical timing under PDI was derived. The critical timing is the timing which maximizes the input energy. The critical timing can be obtained by the time-history response analysis without repetition. Especially in the case of elastic proportionally damped MDOF models, the input energy is maximized when the sum of the first mode inertial forces (equal to the base shear) attains zero.

(4) The distributions of interstory drifts and the distributions of floor accelerations under PDI correspond well to those under the one-cycle sine wave as far as t_0 is close to one half of the fundamental natural period. In the case that t_0 is small, the responses under PDI and the one-cycle sine wave do not correspond well. This is because the one-cycle sine wave excites not only the fundamental-mode response but also the higher-mode responses. In the case that t_0 is large, the higher-mode responses are hardly excited by both PDI and the one-cycle sine wave. However, the responses under PDI are larger than those under the one-cycle sine wave. This is because DI has multiple frequency components and the input energy by PDI exceeds that by the one-cycle sine wave.

(5) The distribution of interstory drifts and the distribution of floor accelerations under the critical PDI correspond well to those under the one-cycle sine wave with t_0 which maximizes the value of $d_{\max}$. As far as the input level is large, the critical timing under PDI and the timing which maximizes the value of $d_{\max}$ under the one-cycle sine wave correspond well. Moreover, the critical timing can be obtained by the time-history response analysis without repetition. Therefore, using the critical PDI helps to efficiently estimate the responses and the input period under the critical one-cycle sine wave for elastic-plastic MDOF models.

(6) The response of elastic-plastic MDOF models under recorded near-fault ground motions was also compared with that under DI, PDI and the one-cycle sine wave. It was shown that the correspondence of the response under PDI and that under the recorded ground motions is fairly good though recorded ground motions are not always critical inputs for elastic-plastic MDOF models. Especially, the floor acceleration response under PDI corresponds well to that under the ground motions while that under DI largely exceed those. The proposed procedure for finding the critical PDI enables the search of the critically modulated recorded ground motions. If we do not use PDI, many repetitive procedures including time-history response analyses are necessary for the recorded ground motions to find the critically time-modulated version of recorded ground motions.

The use of the critical PDI is highly recommended to simulate the acceleration responses, in addition to the deformation responses, under the critical one-cycle sine wave for elastic-plastic MDOF models in place of DI. It is noted that PDI is applicable not only to simple shear frames but also to complicated frame structures. This is because higher-mode responses are hardly excited under the 'critical' one-cycle sine wave in the case that the natural circular frequencies of the higher modes are separated enough from the fundamental natural circular frequency. It is also noted that the influence coefficient vector ι should be modified when the natural circular frequencies of the higher modes are not separated enough from the fundamental natural circular frequency. For example, ι should be modified to $\iota = \alpha_1 \boldsymbol{\varphi}_1 + \alpha_2 \boldsymbol{\varphi}_2$ to treat the critical responses of the buildings with TMD.

Pulse-like motions may cause devastating damage to building structures. Especially, the plastic deformation concentration to specific stories must be prevented for the safety of buildings and human lives. The simulation of the critical elastic-plastic responses of buildings under pulse-like motions by PDI will help to design safer buildings by capturing simultaneously the resonant deformation and acceleration responses without repetitive procedures for finding the resonant period.

8. Acknowledgement

Part of the present work is supported by the Grant-in-Aid for Scientific Research (KAKENHI) of Japan Society for the Promotion of Science (No.18H01584, JP20J20811). This support is greatly appreciated.

9. References

[1] Bertero, V. V., Mahin, S. A., and Herrera, R. A. Aseismic design implications of near-fault San Fernando earthquake records. *Earthq. Eng. Struct. Dyn*., 1978, 6(1), 31–42.

[2] Sasani, M., and Bertero, V. V. Importance of severe pulse-type ground motions in performance-based engineering: Historical and critical. In *Proc. of the 12th World Conf. on Earthq. Eng., New Zealand Society for Earthq. Eng., Upper Hutt, New Zealand*, 2000.

[3] Takewaki, I., Murakami, S., Fujita, K., Yoshitomi, S., and Tsuji, M. The 2011 off the Pacific coast of Tohoku earthquake and response of high-rise buildings under long-period ground motions. *Soil Dyn. Earthq. Eng*., 2011, 31(11), 1511-1528.

[4] Mavroeidis, G. P., and Papageorgiou, A. S. A mathematical representation of near-fault ground motions. *Bull. Seism. Soc. Am*., 2003, 93(3), 1099-1131.

[5] Baker, J. W. Quantitative classification of near-fault ground motions using wavelet analysis. *Bull. Seism. Soc. Am*., 2007, 97(5), 1486-1501.

[6] Makris, N., and Black, C. J. Dimensional analysis of rigid-plastic and elastoplastic structures under pulse-type excitations. *J. Eng. Mech*., 2004, 130(9), 1006-1018.

[7] Kalkan, E., and Kunnath, S. K. Effects of fling step and forward directivity on seismic response of buildings, *Earthq. Spectra*, 2006, 22(2), 367–390.

[8] Hayden, C. P., Bray, J. D., and Abrahamson, N. A. Selection of near-fault pulse motions. *J. Geotech. Geoenviron. Eng*., 2014, 140(7), 04014030.

[9] Akehashi, H., Kojima, K., Farsangi, E. N., and Takewaki, I. Critical response evaluation of damped bilinear hysteretic SDOF model under long duration ground motion simulated by multi impulse motion. *Int. J. Earthq. Impact Eng*., 2018, 2(4), 298-321.

[10] Akehashi, H. and Takewaki, I. Optimal viscous damper placement for elastic-plastic MDOF structures under critical double impulse. *Frontiers in Built Environment*, 2019, 5: 20.

[11] Akehashi, H. and Takewaki, I. Comparative investigation on optimal viscous damper placement for elastic-plastic MDOF structures: Transfer function amplitude or double impulse. *Soil Dyn. Earthq. Eng*., 2020, 130, 105987.

[12] Akehashi, H., and Takewaki, I. Simultaneous optimization of elastic-plastic building structures and viscous dampers under critical double impulse. *Frontiers in Built Environment*, 2020, 6: 211.

[13] Tirca, L. D., Foti, D., and Diaferio, M. Response of middle-rise steel frames with and without passive dampers to near-field ground motions. *Eng. Struct*., 2003, 25(2), 169-179.

[14] Bray, J. D., and Rodriguez-Marek, A. Characterization of forward-directivity ground motions in the near-fault region. *Soil Dyn. Earthq. Eng*., 2004, 24(11), 815-828.

[15] Gicev, V., and Trifunac, M. D. Permanent deformations and strains in a shear building excited by a strong motion pulse. *Soil Dyn. Earthq. Eng*., 2007, 27(8), 774-792.

[16] Yang, D., Pan, J., and Li, G. Interstory drift ratio of building structures subjected to near-fault ground motions based on generalized drift spectral analysis. *Soil Dyn. Earthq. Eng*., 2010, 30(11), 1182-1197.

[17] Alonso-Rodríguez, A., and Miranda, E. Assessment of building behavior under near-fault pulse-like ground motions through simplified models. *Soil Dyn. Earthq. Eng*., 2015, 79, 47-58.

[18] Durucan, C., and Durucan, A. R. Ap/Vp specific inelastic displacement ratio for the seismic response estimation of SDOF structures subjected to sequential near fault pulse type ground motion records. *Soil Dyn. Earthq. Eng*., 2016, 89, 163-170.

[19] Yadav, K. K., and Gupta, V. K. Near-fault fling-step ground motions: characteristics and simulation. *Soil Dyn. Earthq. Eng*., 2017, 101, 90-104.

[20] Pu, W., Wu, M., Huang, B., and Zhang, H. Quantification of response spectra of pulse-like near-fault ground motions. *Soil Dyn. Earthq. Eng*., 2018, 104, 117-130.

[21] Masaeli, H., Khoshnoudian, F., and Musician, S. Incremental dynamic analysis of nonlinear rocking soil-structure systems. *Soil Dyn. Earthq. Eng*., 2018, 104, 236-249.

[22] Ji, K., Ren, Y., Wen, R., and Kuo, C. H. Near-field velocity pulse-like ground motions on February 6, 2018 MW6. 4 Hualien, Taiwan earthquake and structural damage implications. *Soil Dyn. Earthq. Eng*., 2019, 126, 105784.

[23] Li, C., Zuo, Z., Kunnath, S., and Chen, L. Orientation of the strongest velocity pulses and the maximum structural response to pulse-like ground motions. *Soil Dyn. Earthq. Eng*., 2020, 136, 106240.

[24] Drenick, R. F. Model-free design of aseismic structures. *J. Eng. Mech. Div*., 1970, 96(4), 483-493.

[25] Iyengar, R. N., and Manohar, C. S. Nonstationary random critical seismic excitations. *J. Eng. Mech.*, 1987, 113(4), 529-541.

[26] Takewaki, I. *Critical excitation methods in earthquake engineering*. 2013, Butterworth-Heinemann.

[27] Kojima, K., and Takewaki, I. Critical earthquake response of elastic-plastic structures under near-fault ground motions (Part 1: Fling-step input), *Frontiers in Built Environment*, 2015, 1: 12.

[28] Kojima, K., and Takewaki, I. Critical input and response of elastic–plastic structures under long-duration earthquake ground motions. *Frontiers in Built Environment*, 2015, 1: 15.

[29] Taniguchi, R., Kojima, K., and Takewaki, I. Critical response of 2DOF elastic–Plastic Building structures under Double impulse as substitute of near-Fault ground motion. *Frontiers in Built Environment*, 2016, 2: 2.

[30] Shiomi, T., Fujita, K., Tsuji, M., and Takewaki, I. Dual hysteretic damper system effective for broader class of earthquake ground motions. *Int. J. Earthq. Impact Eng.*, 2018, 2(3), 175-202.

[31] Ishida, S. and Takewaki, I. Optimal seismic design of stiffness and gap of hysteretic-viscous hybrid damper system in nonlinear building frames for simultaneous reduction of interstory drift and acceleration. *Frontiers in Built Environment*, 2021, 7: 656606.

[32] Rodriguez, M. E., Restrepo, J. I. and Carr, A. J. Earthquake-induced floor horizontal accelerations in buildings. *Earthq. Eng. Struct. Dyn.*, 2002, 31, 693-718.

[33] Vukobratović, V., and Fajfar, P. A method for the direct estimation of floor acceleration spectra for elastic and inelastic MDOF structures. *Earthq. Eng. Struct. Dyn.*, 2016, 45(15), 2495-2511.

[34] Skinner, R. I., Robinson, W. H., and McVerry, G. H. *An introduction to seismic isolation*. 1993, Wiley.

[35] Kojima, K., and Takewaki, I. Closed-form critical earthquake response of elastic-plastic structures with bilinear hysteresis under near-fault ground motions. *J. Struct. Construct. Eng.*, 2016, 726, 1209–1219 (in Japanese).

Appendix 1: Transfer function of acceleration

Figure A1 shows the transfer functions $H_{a,N}^{g}$ of the absolute accelerations at the top story with respect to input ground acceleration and the transfer functions $H_{a,N}^{f}$ of the 'relative' (to ground) accelerations at the top story with respect to lateral force input with $\boldsymbol{\iota} = \alpha_1 \boldsymbol{\varphi}_1$. The latter transfer function is the ratio of the relative acceleration at the top story with respect to $V\delta(t) - V\delta(t - t_0)$ in Eq.(20). It can be observed that higher modes hardly contribute to $H_{a,N}^{f}$ and the values of $H_{a,N}^{f}$ at $\omega = 0$ are zero due to the absence of the ground motion. Although the components of $H_{a,N}^{f}$ in a higher frequency range are thought to enlarge the acceleration responses under PDI, this is not true. These components correspond to the Dirac delta function in time domain since the real parts of these components are almost constant and the imaginary parts are almost 0. In other words, an impulsive lateral force causes impulsive relative acceleration responses. Such impulsive acceleration responses are excluded in the evaluation of the maximum acceleration responses. This fact supports the validity of using PDI in the evaluation of acceleration in place of DI.

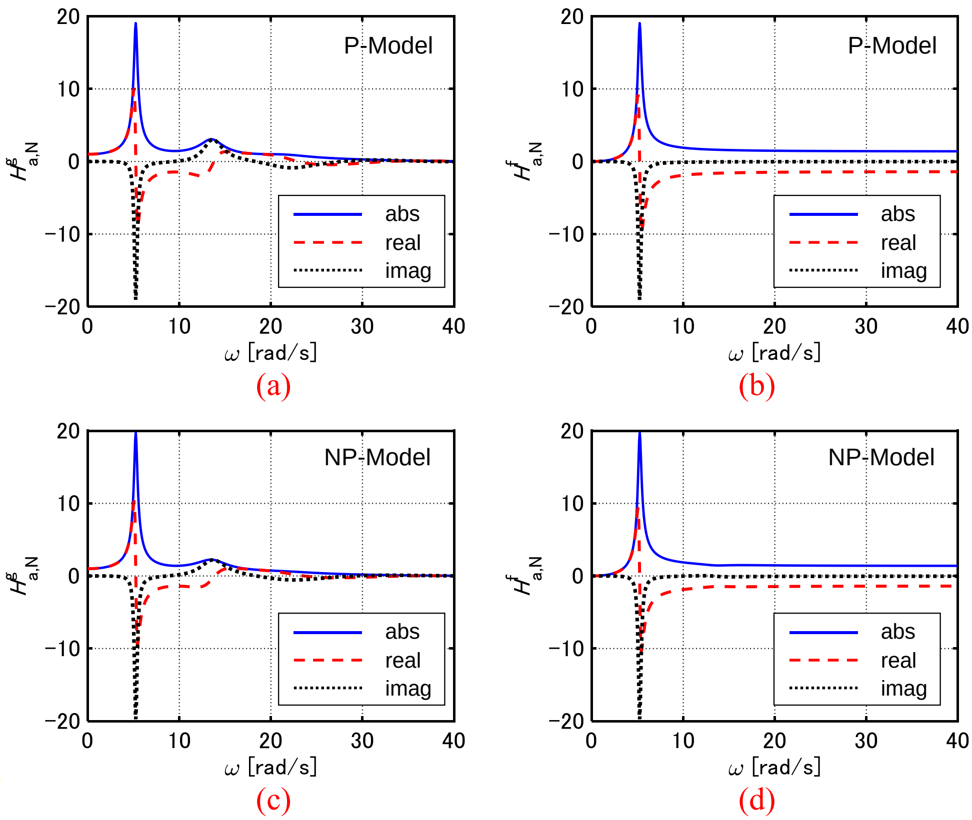

Figure A1 Transfer functions $H^g_{a,N}$ of absolute acceleration at top story with respect to input ground acceleration and transfer functions $H^f_{a,N}$ of relative acceleration at top story with respect to lateral force input with $\boldsymbol{\iota} = \alpha_1 \boldsymbol{\varphi}_1$, (a) $H^g_{a,N}$ of P-Model, (b) $H^f_{a,N}$ of P-Model, (c) $H^g_{a,N}$ of NP-Model, (d) $H^f_{a,N}$ of NP-Model

Appendix 2: Phase properties of maximum responses

The phase properties corresponding to the maximum responses under PDI are derived for proportionally damped elastic MDOF models. Figure A2 illustrates the phases of the maximum responses under the critical PDI in the complex plane. The timing $t_{d,1}$ at which the displacement response attains the maximum under the 1st impulse of the critical PDI is the timing at which the velocity response attains 0. $t_{d,1}$ is expressed as follows.

$$t_{d,1} = \{(\pi/2) - \phi_1\}/\omega_{D1} \tag{A1}$$

In the same way, the timing $t_{v,1}$ at which the velocity response attains the maximum under the 1st impulse of the critical PDI and the timing $t_{a,1}$ at which the acceleration response attains the maximum are derived as

$$t_{v,1} = (\pi - 2\phi_1)/\omega_{D1} \tag{A2}$$

$$t_{a,1} = \{(\pi/2) - 3\phi_1\}/\omega_{D1} \tag{A3}$$

The timings $t_{d,2}, t_{v,2}, t_{a,2}$ at which the displacement, velocity and acceleration responses attain the maximum under the 2nd impulse of the critical PDI are derived as follows.

$$t_{d,2} = t_0^c + \{(\pi/2) - (\hat{\phi}_1 - \phi_1)\} / \omega_{D1} \quad \text{(A4)}$$

$$t_{v,2} = t_0^c + (\pi - \hat{\phi}_1) / \omega_{D1} \quad \text{(A5)}$$

$$t_{a,2} = t_0^c + \{(\pi/2) - (\hat{\phi}_1 + \phi_1)\} / \omega_{D1} \quad \text{(A6)}$$

where $\hat{\phi}_1$ is the phase angle between $\ddot{u}$ and the imaginary axis, and $\hat{\phi}_1$ is expressed by

$$\hat{\phi}_1 = \arctan \frac{\sin(2\phi_1)}{\cos(2\phi_1) + \exp(-h_1 \omega_1 t_0^c)} \quad \text{(A7)}$$

$\hat{\phi}_1$ satisfies $\phi_1 < \hat{\phi}_1 < 2\phi_1$. By substituting Equations (A1-A6) into Equations (22a, b), (23a, b), the maximum responses under the critical PDI are evaluated.

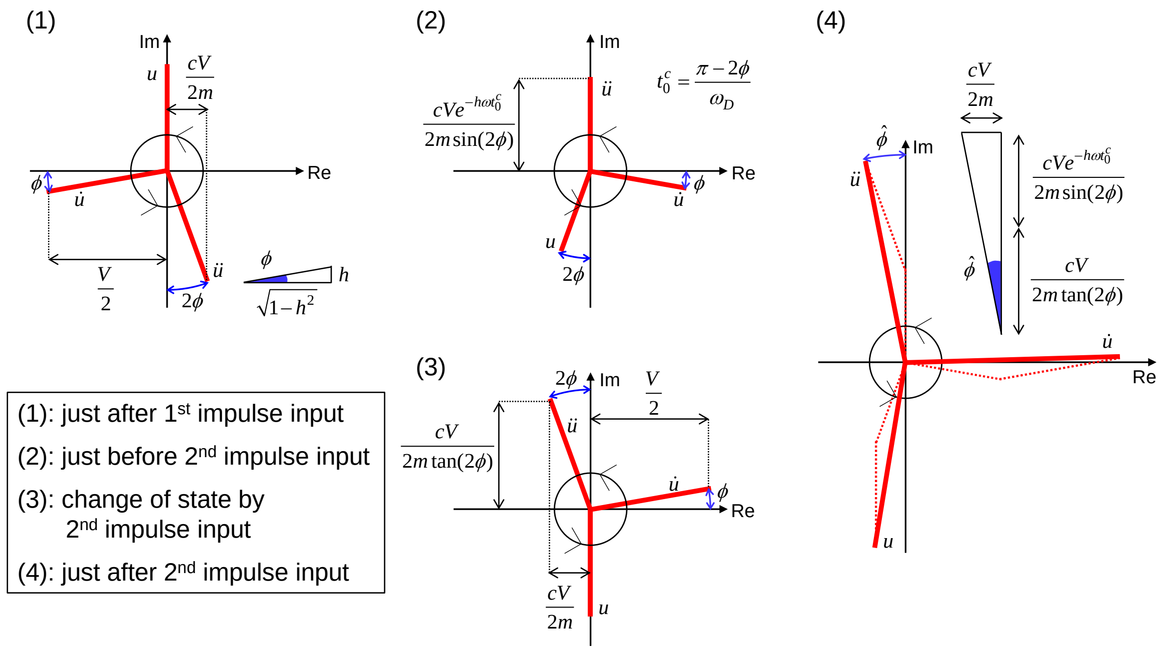

Figure A2 Phases of responses under critical PDI in complex plane

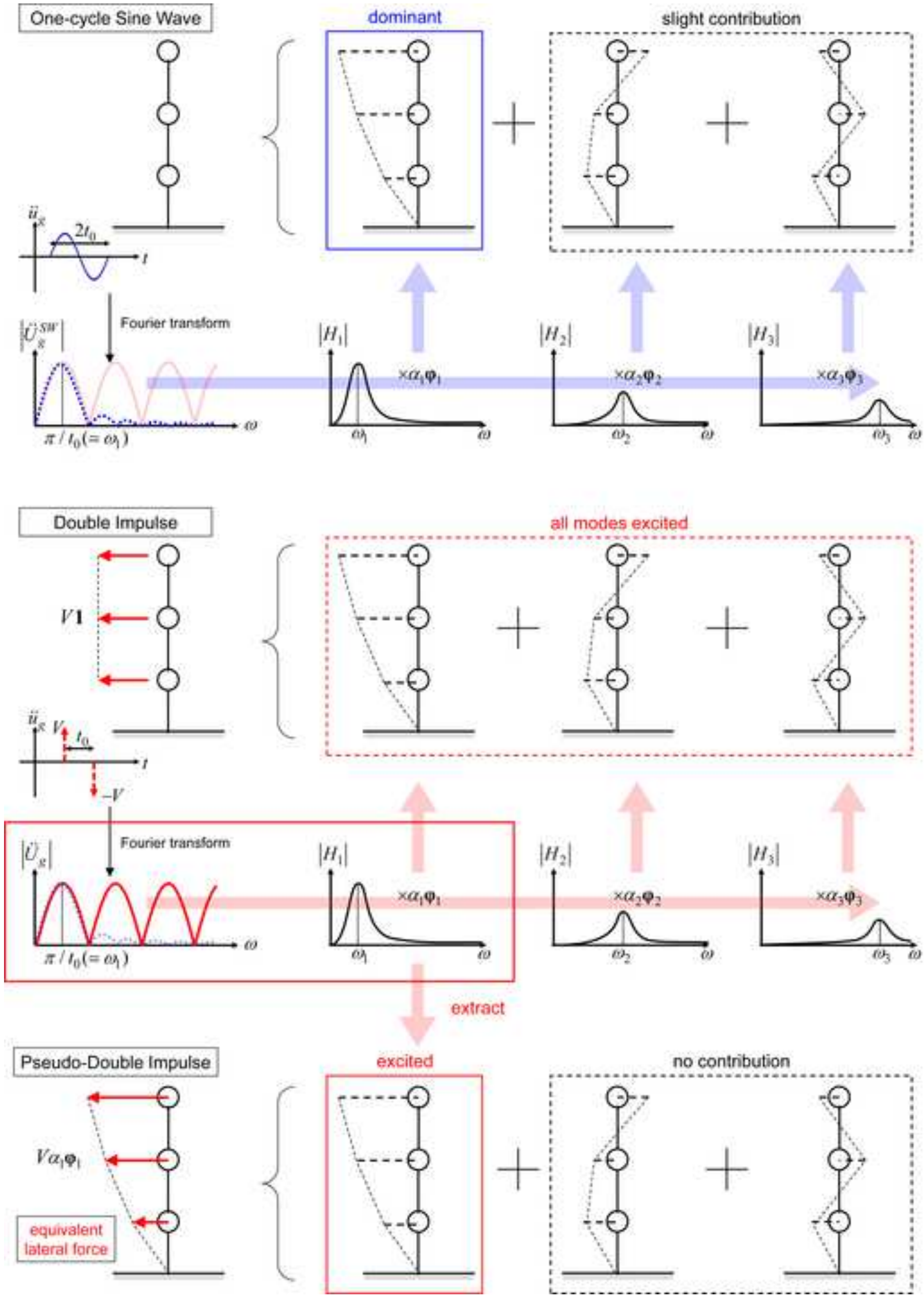

One-cycle Sine Wave
dominant
slight contribution
$2t_0$
Fourier transform
$|H_1|$
$|H_2|$
$|H_3|$
$\times\alpha_1\varphi_1$
$\times\alpha_2\varphi_2$
$\times\alpha_3\varphi_3$
$\pi / t_0 (= \omega_1)$
Double Impulse
all modes excited
$V\mathbf{1}$
t_0
$-V$
Fourier transform
extract
Pseudo-Double Impulse
excited
no contribution
$V\alpha_1\varphi_1$
equivalent lateral force

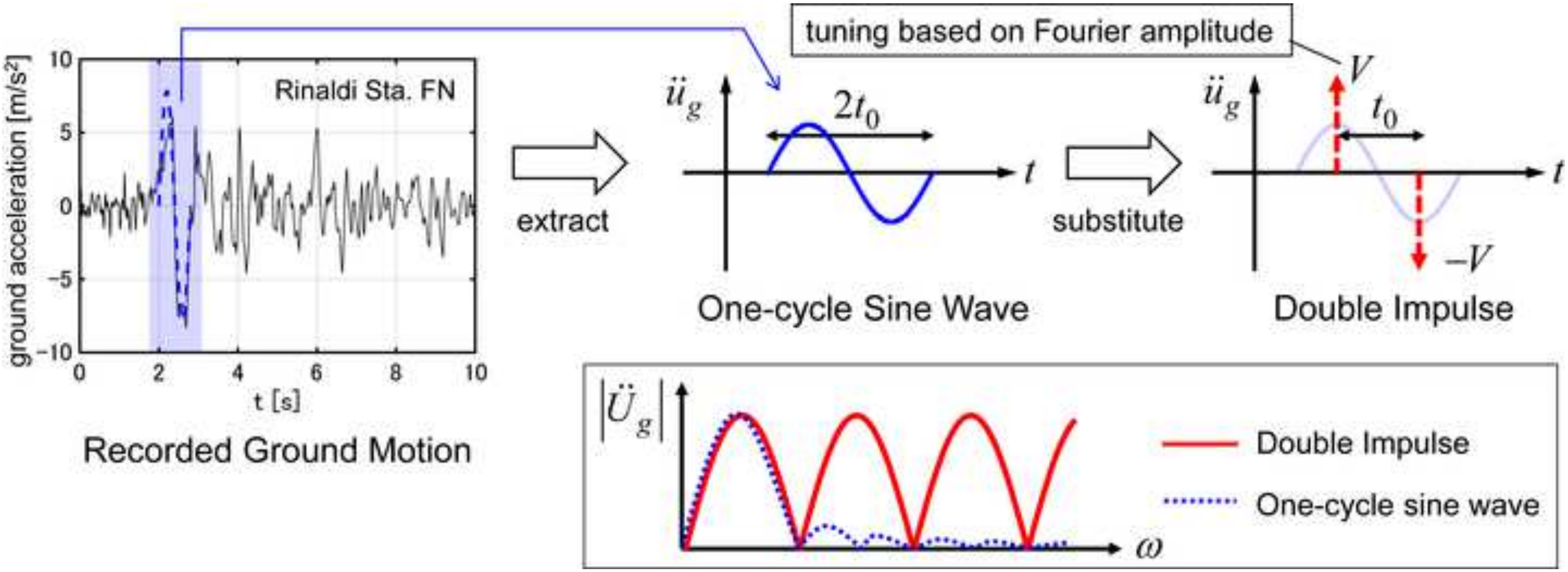

Rinaldi Sta. FN
ground acceleration [m/s²]
t [s]
Recorded Ground Motion
extract
$\ddot{u}_g$
$2t_0$
t
One-cycle Sine Wave
substitute
tuning based on Fourier amplitude
V
t_0
$-V$
Double Impulse
$|\ddot{U}_g|$
ω
Double Impulse
One-cycle sine wave

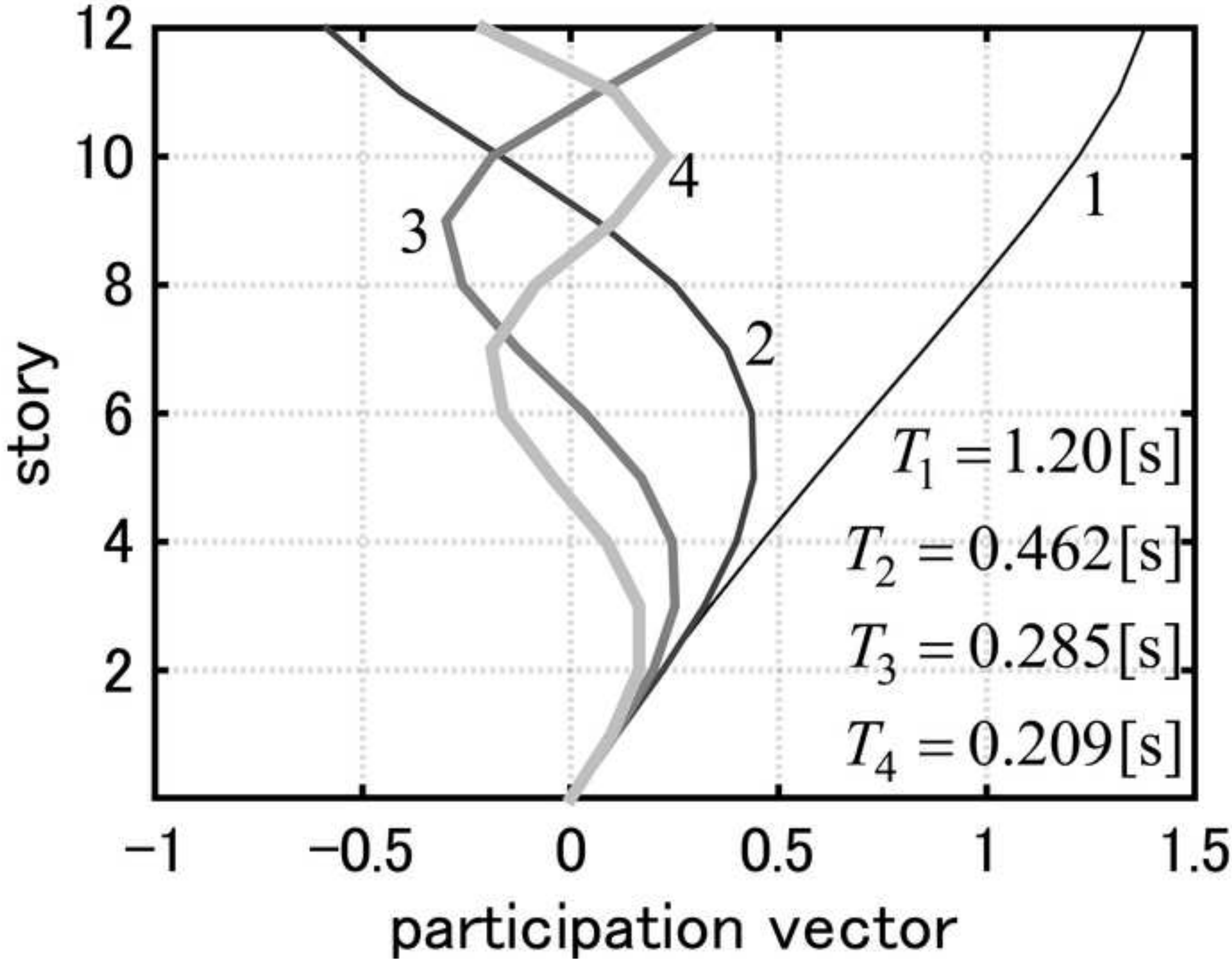
12
10
8
6
4
2
story
−1
−0.5
0
0.5
1
1.5
participation vector
1
2
3
4
$T_1 = 1.20$[s]
$T_2 = 0.462$[s]
$T_3 = 0.285$[s]
$T_4 = 0.209$[s]

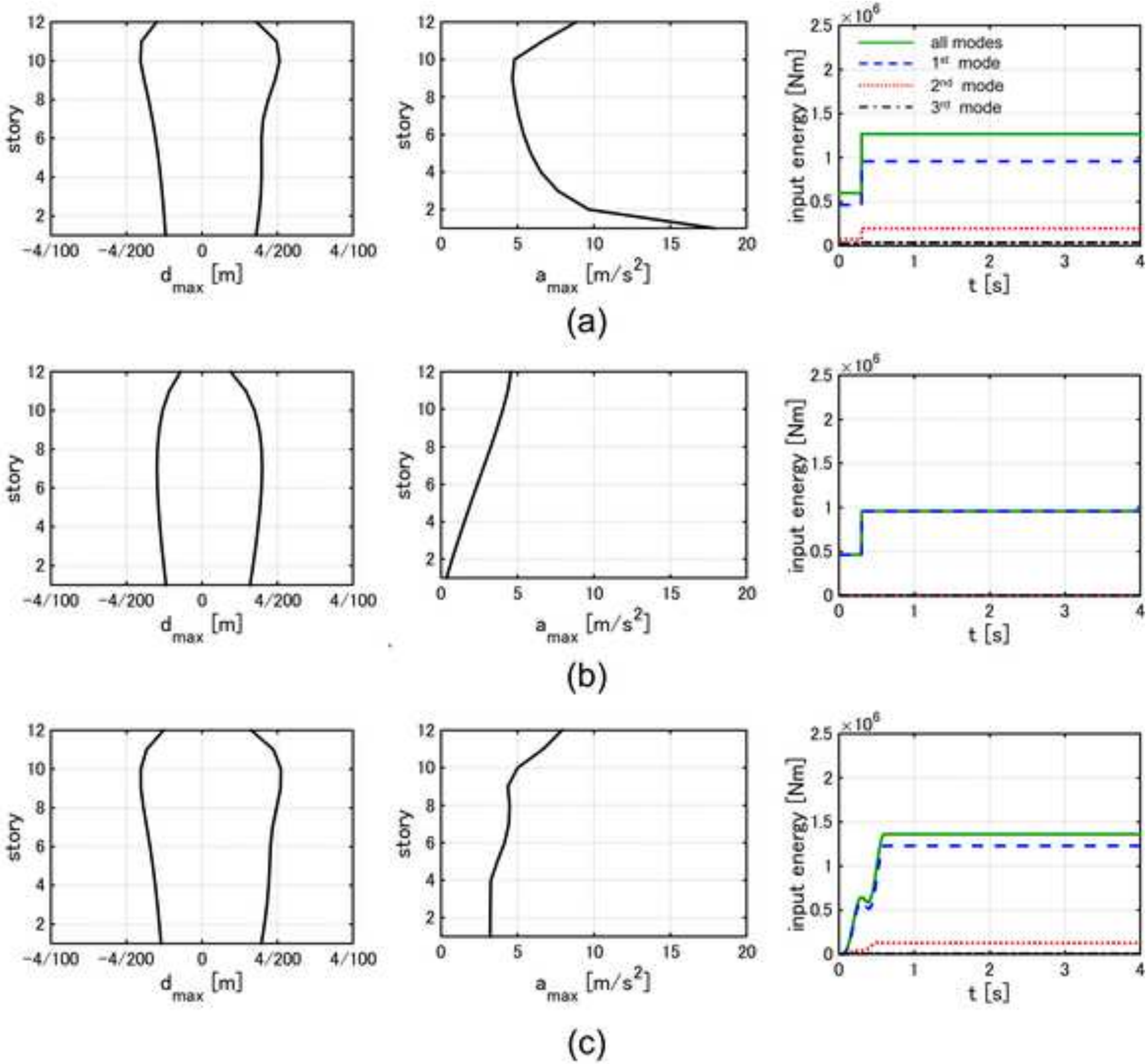
story
d_{max} [m]
−4/100
−4/200
0
4/200
4/100
story
a_{max} [m/s^2]
input energy [Nm]
$\times 10^6$
all modes
1st mode
2nd mode
3rd mode
t [s]
(a)
(b)
(c)

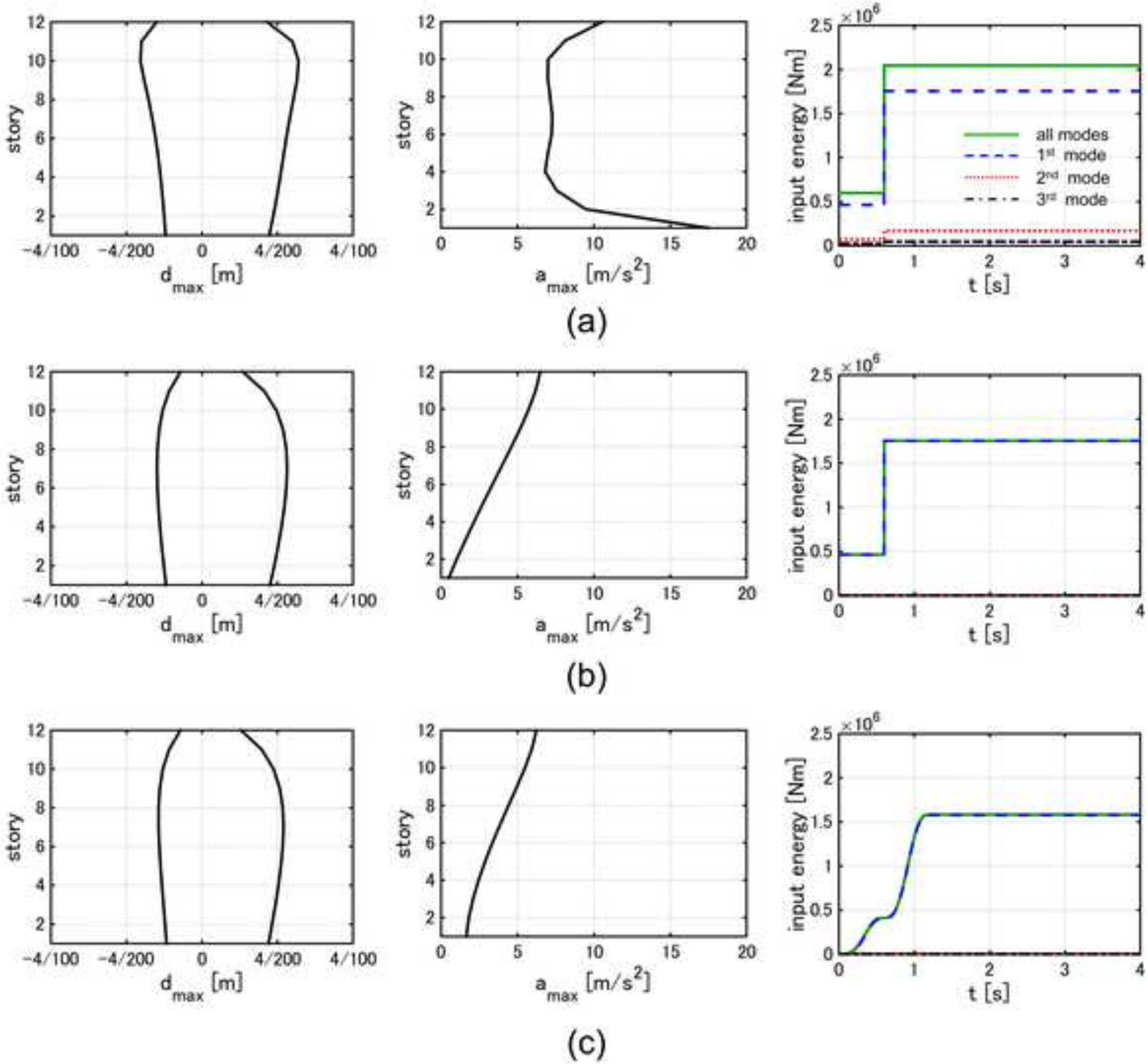

story
d max [m]
-4/100
-4/200
0
4/200
4/100
a max [m/s2]
input energy [Nm]
×10^6
t [s]
all modes
1st mode
2nd mode
3rd mode
(a)
(b)
(c)

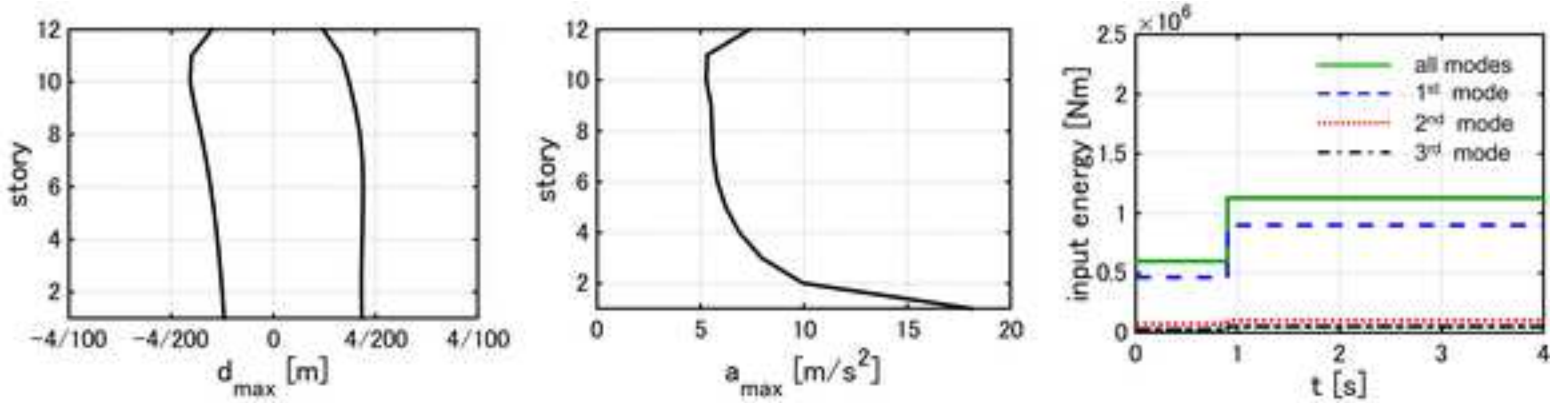
story
d_{max} [m]
−4/100
−4/200
0
4/200
4/100
a_{max} [m/s^2]
input energy [Nm]
×10^6
t [s]
all modes
1st mode
2nd mode
3rd mode

(a)

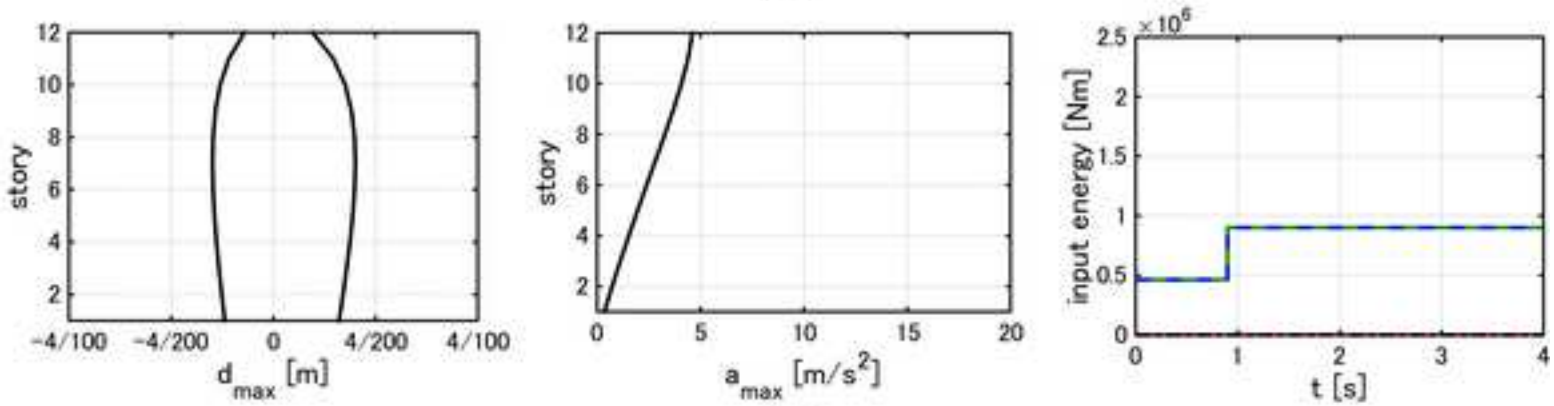
story
d_{max} [m]
a_{max} [m/s^2]
input energy [Nm]
×10^6
t [s]

(b)

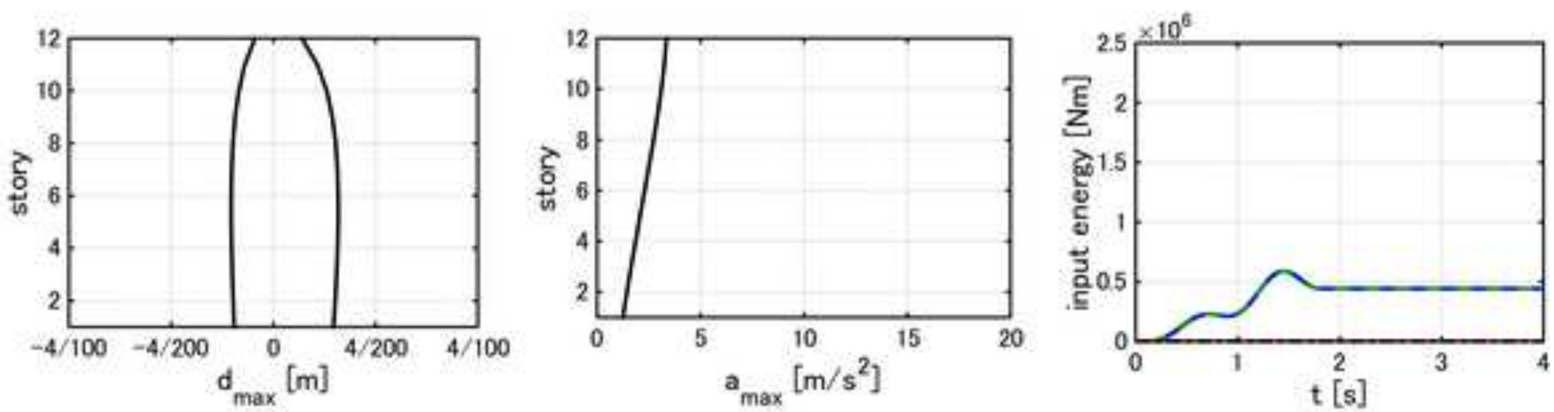
story
d_{max} [m]
a_{max} [m/s^2]
input energy [Nm]
×10^6
t [s]

(c)

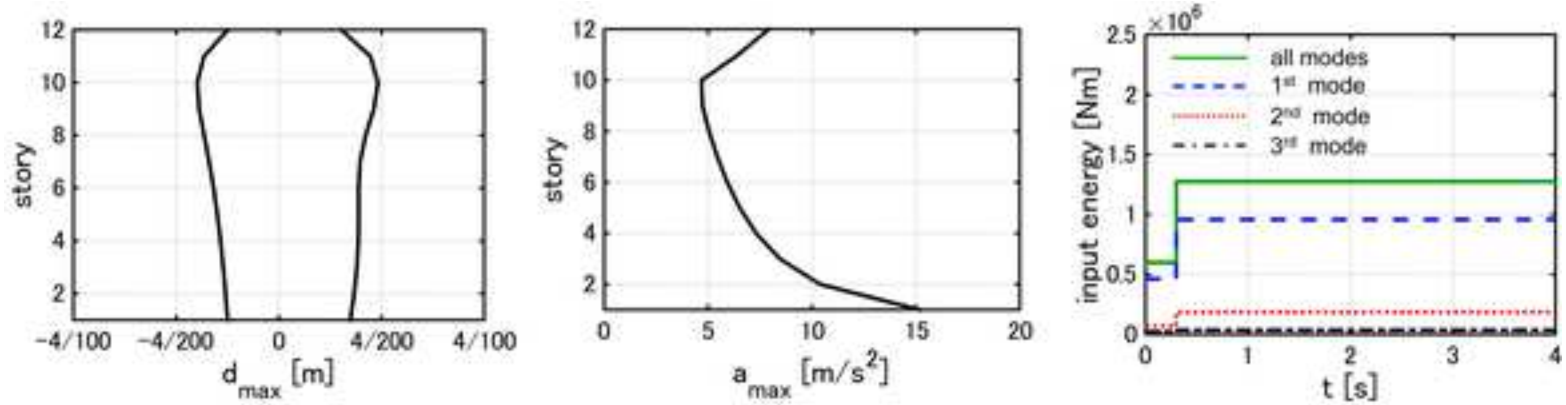

story
d_{max} [m]
−4/100
−4/200
0
4/200
4/100
a_{max} [m/s^2]
input energy [Nm]
$\times 10^6$
t [s]
all modes
1st mode
2nd mode
3rd mode

(a)

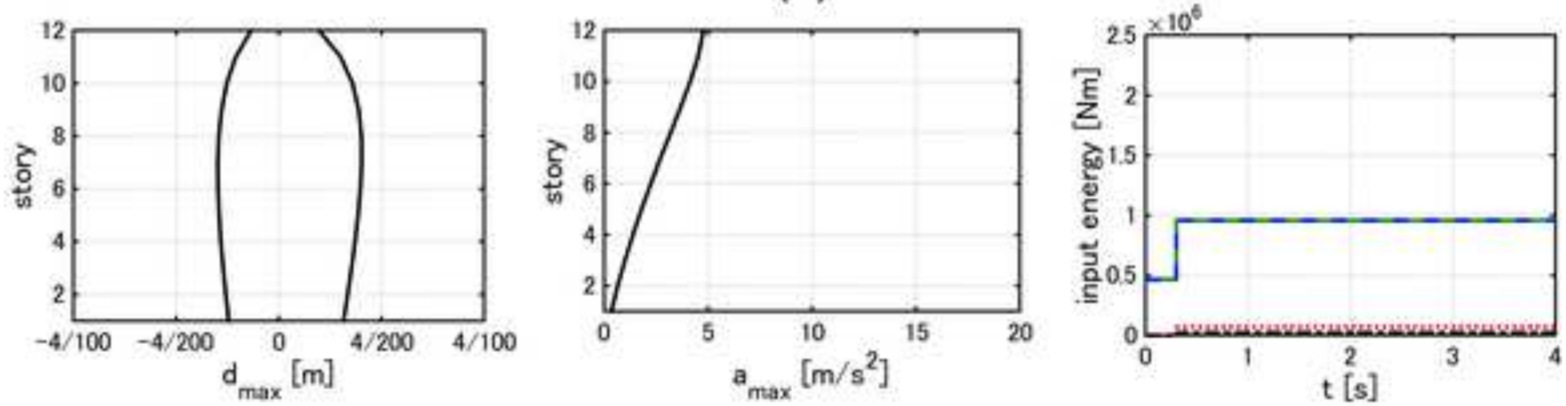

story
d_{max} [m]
−4/100
−4/200
0
4/200
4/100
a_{max} [m/s^2]
input energy [Nm]
$\times 10^6$
t [s]

(b)

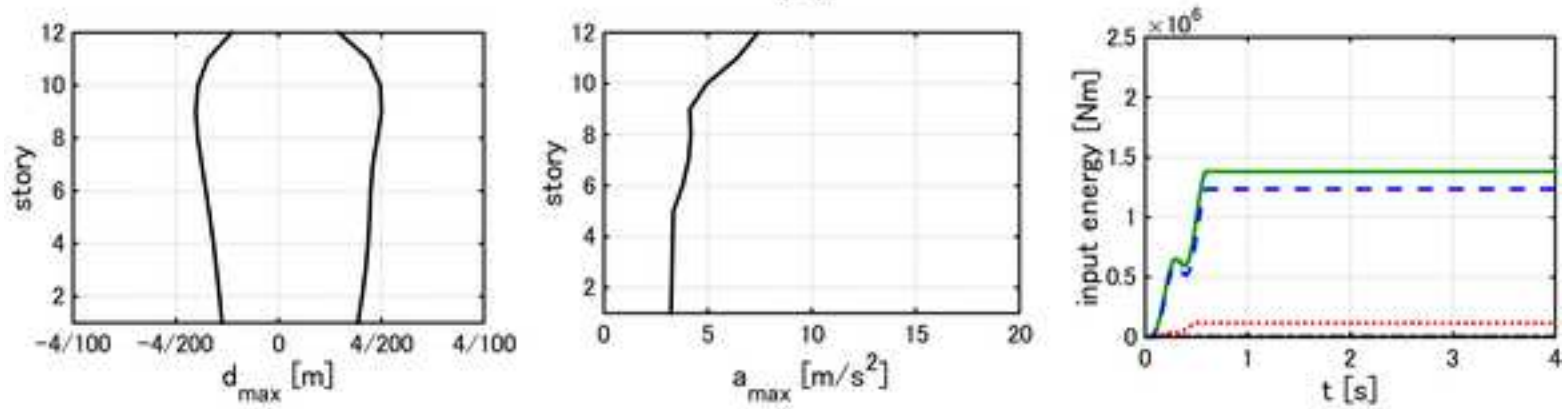

story
d_{max} [m]
−4/100
−4/200
0
4/200
4/100
a_{max} [m/s^2]
input energy [Nm]
$\times 10^6$
t [s]

(c)

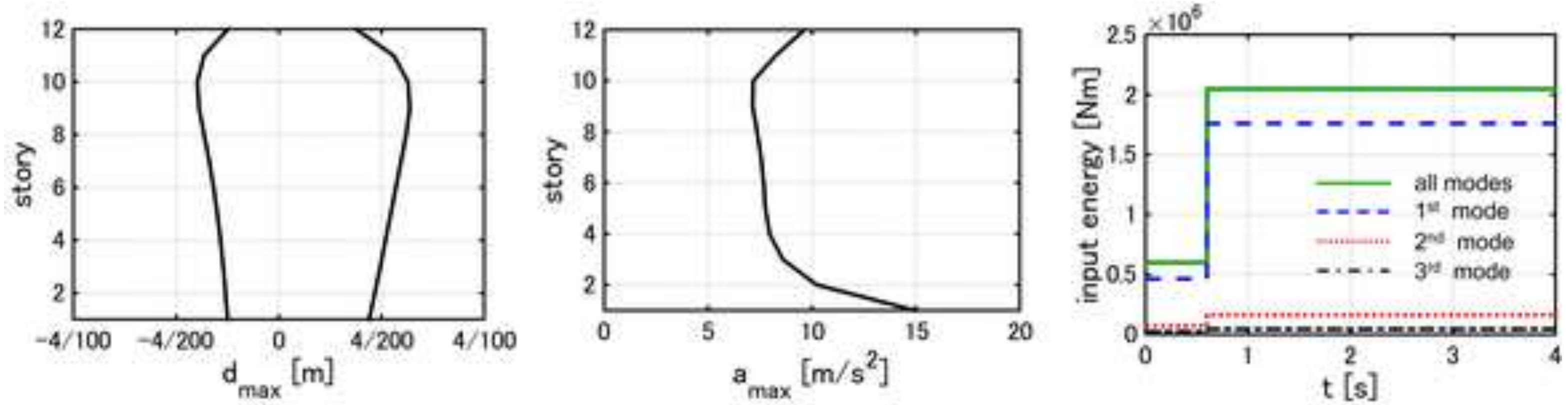
story
d_{max} [m]
−4/100 −4/200 0 4/200 4/100
a_{max} [m/s^2]
input energy [Nm]
$\times 10^6$
all modes
1st mode
2nd mode
3rd mode
t [s]

(a)

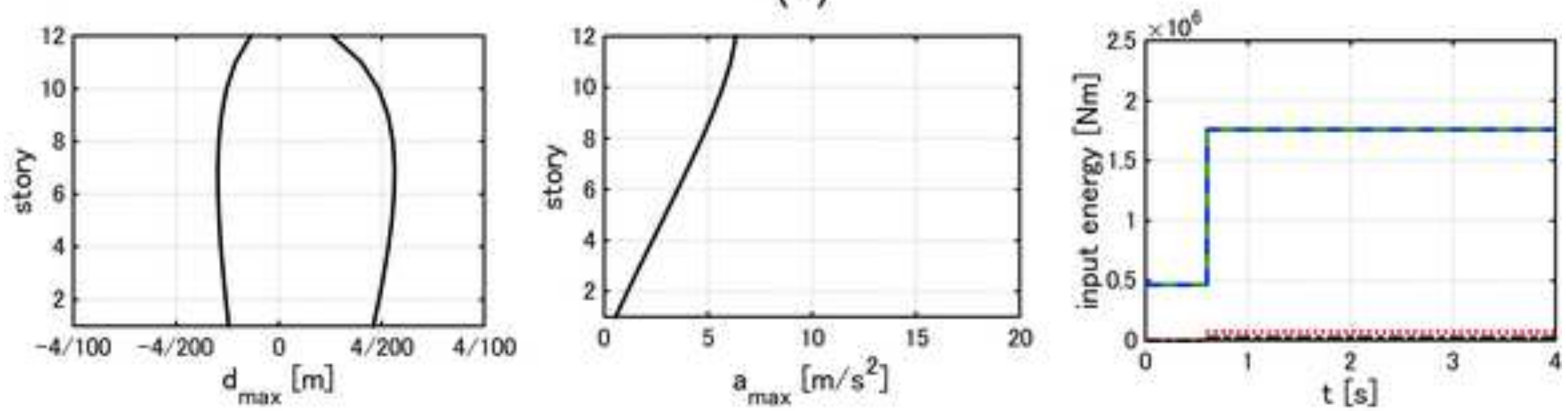
story
d_{max} [m]
−4/100 −4/200 0 4/200 4/100
a_{max} [m/s^2]
input energy [Nm]
$\times 10^6$
t [s]

(b)

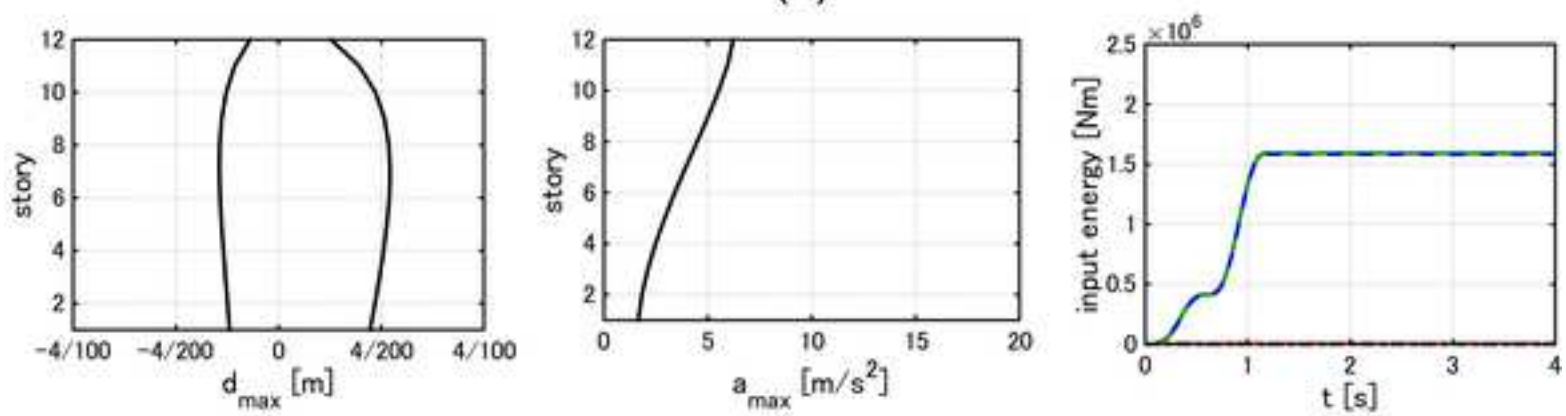
story
d_{max} [m]
−4/100 −4/200 0 4/200 4/100
a_{max} [m/s^2]
input energy [Nm]
$\times 10^6$
t [s]

(c)

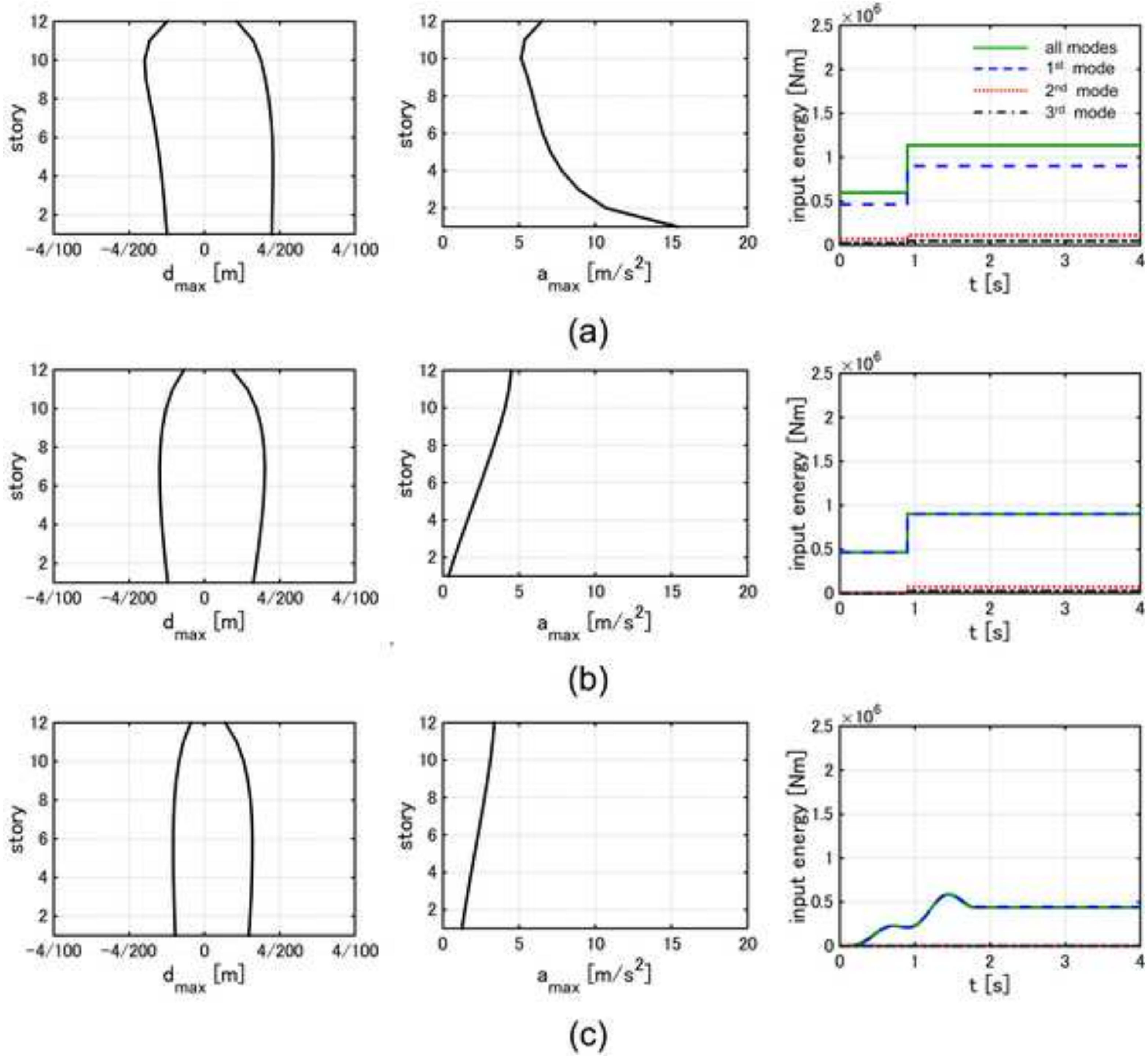
story
d_{max} [m]
−4/100
−4/200
0
4/200
4/100
a_{max} [m/s^2]
input energy [Nm]
$\times 10^6$
t [s]
all modes
1st mode
2nd mode
3rd mode
(a)
(b)
(c)

Click here to access/download;Figure;Fig10.tif

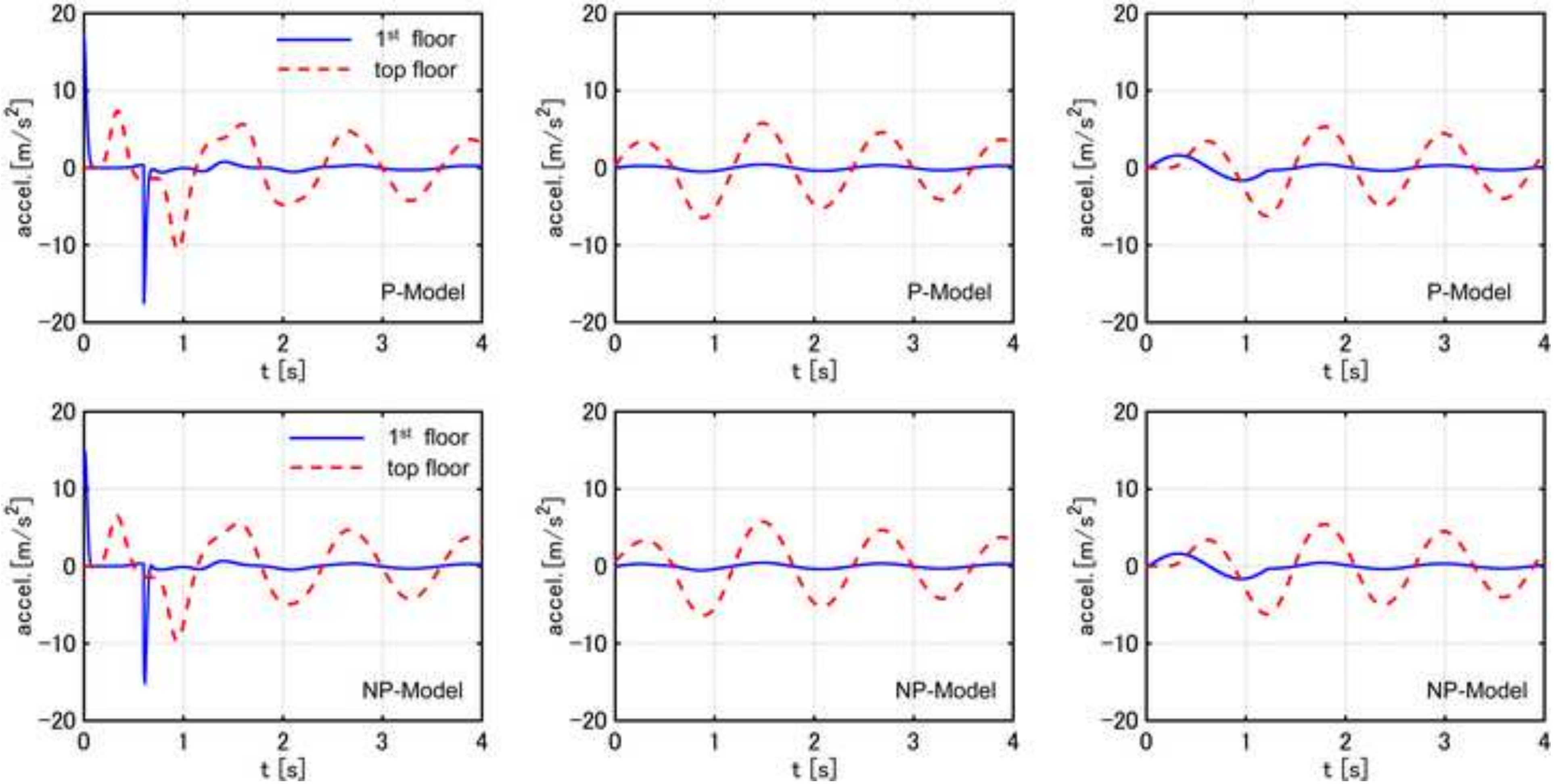

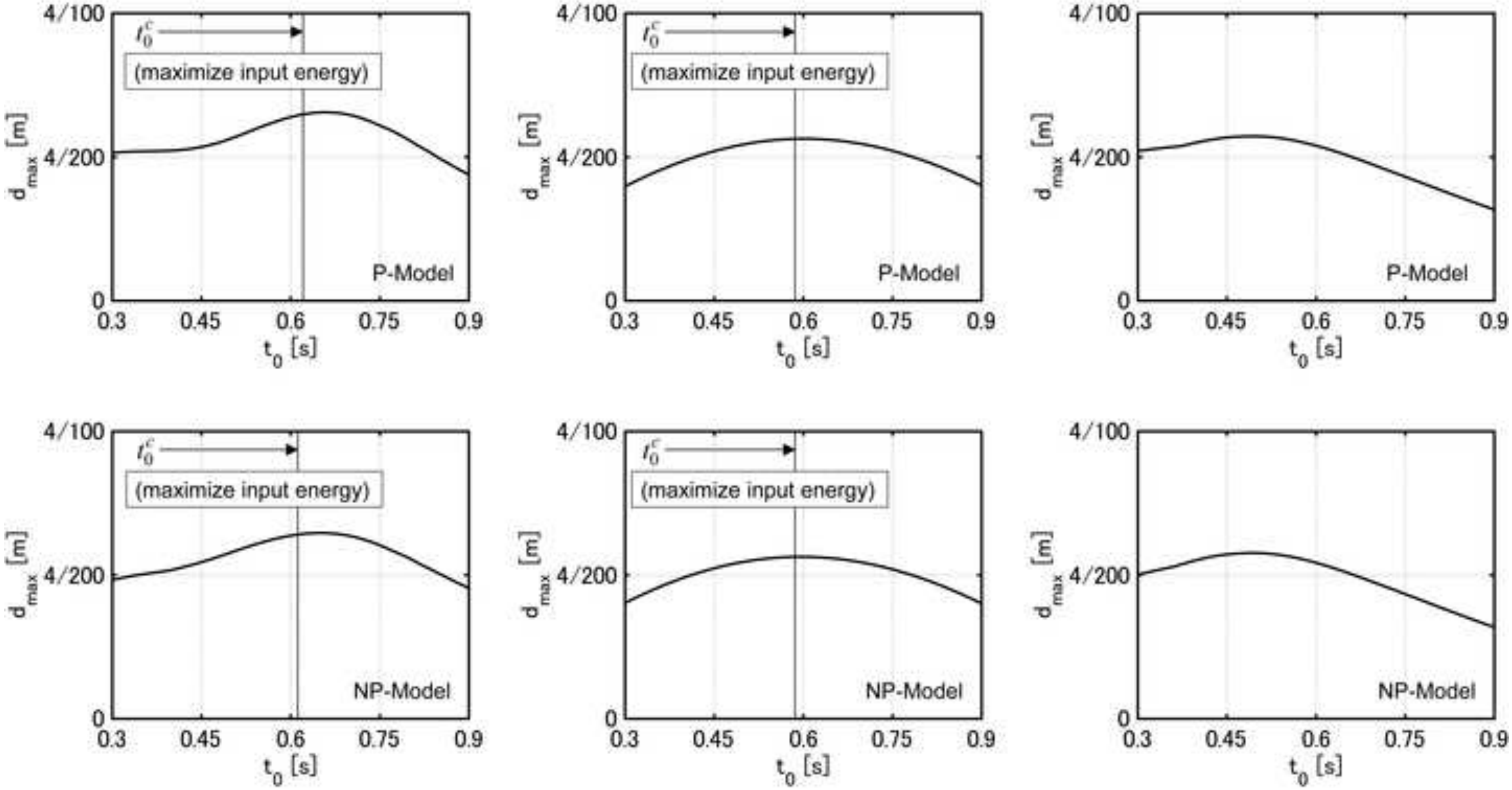

4/100
4/200
0
0.3
0.45
0.6
0.75
0.9
d_{max} [m]
t_0 [s]
t_0^c
(maximize input energy)
P-Model
NP-Model

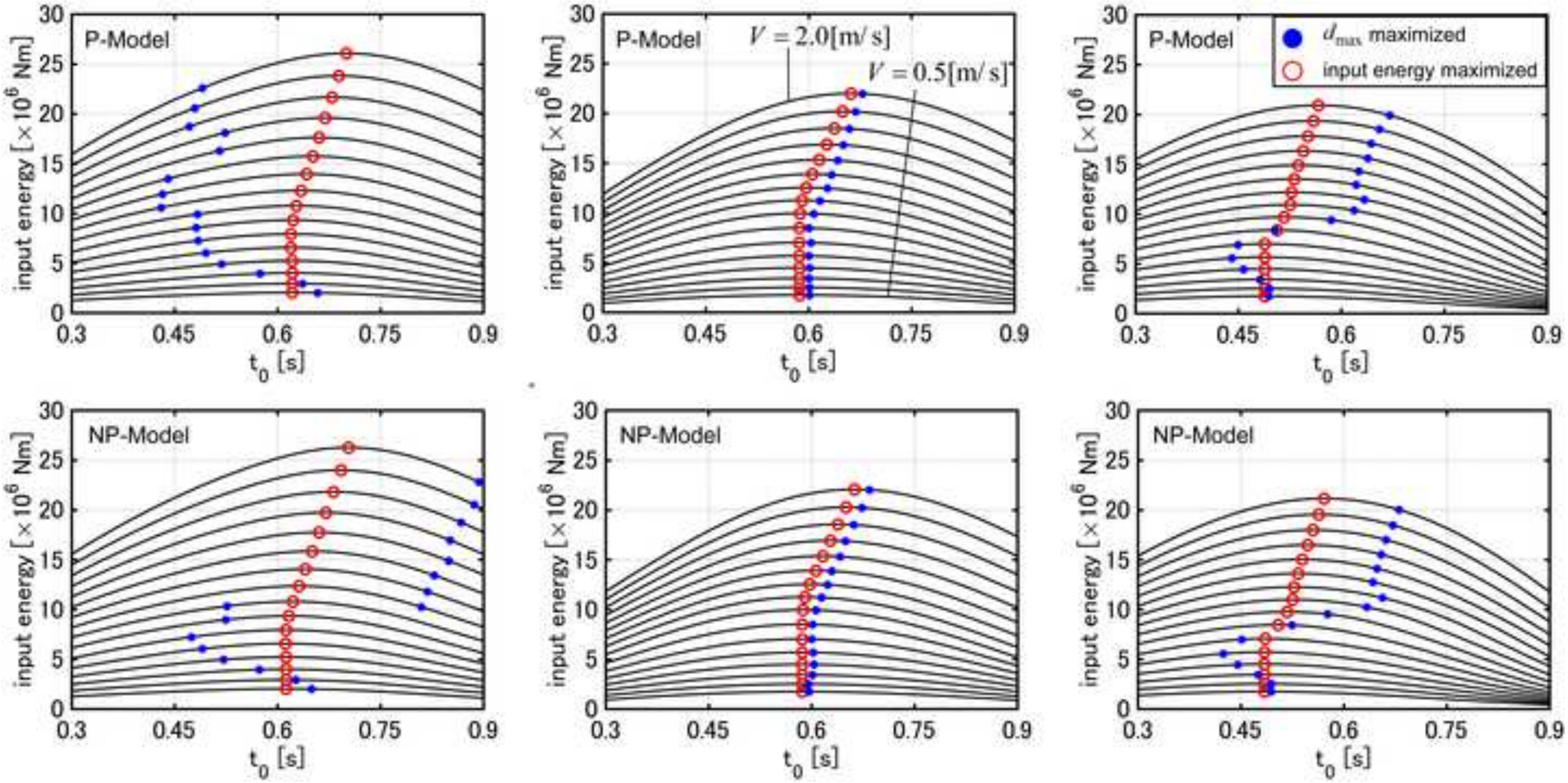
P-Model
NP-Model
$V = 2.0$[m/s]
$V = 0.5$[m/s]
d_{max} maximized
input energy maximized
input energy [$\times 10^6$ Nm]
t_0 [s]

Click here to access/download;Figure;Fig13.tif

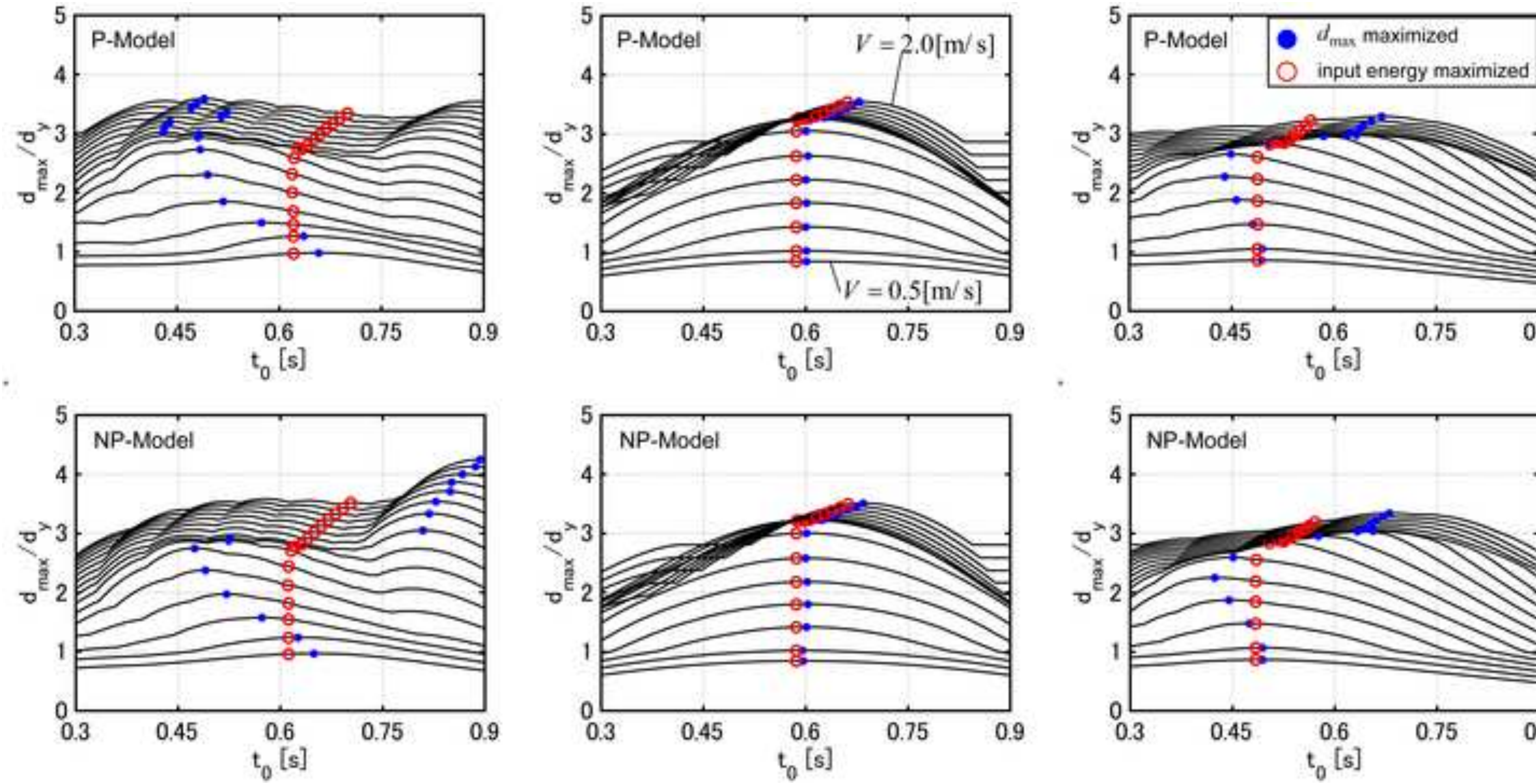

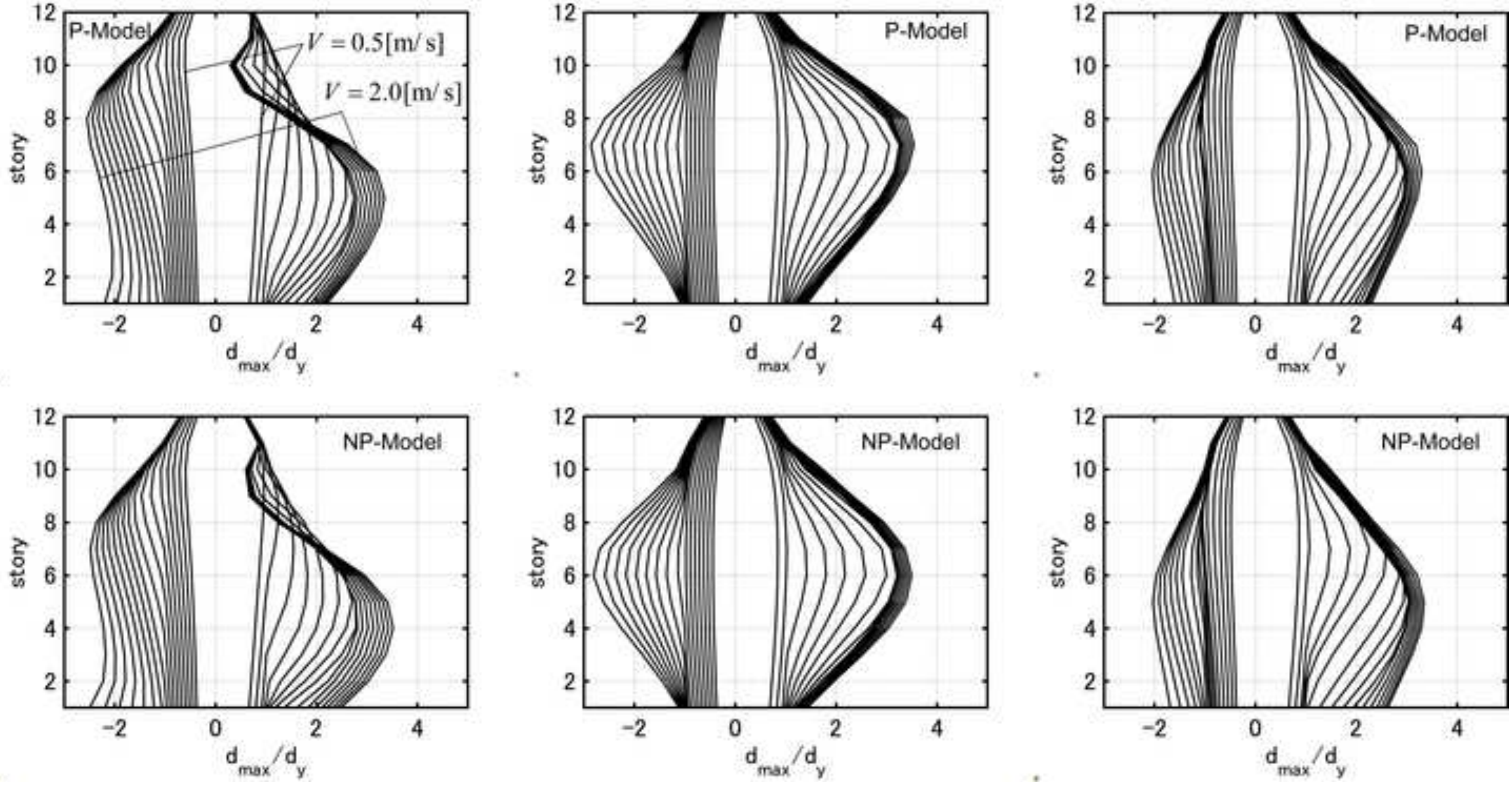
P-Model
$V = 0.5$[m/s]
$V = 2.0$[m/s]
P-Model
P-Model
NP-Model
NP-Model
NP-Model
story
d_{max}/d_y

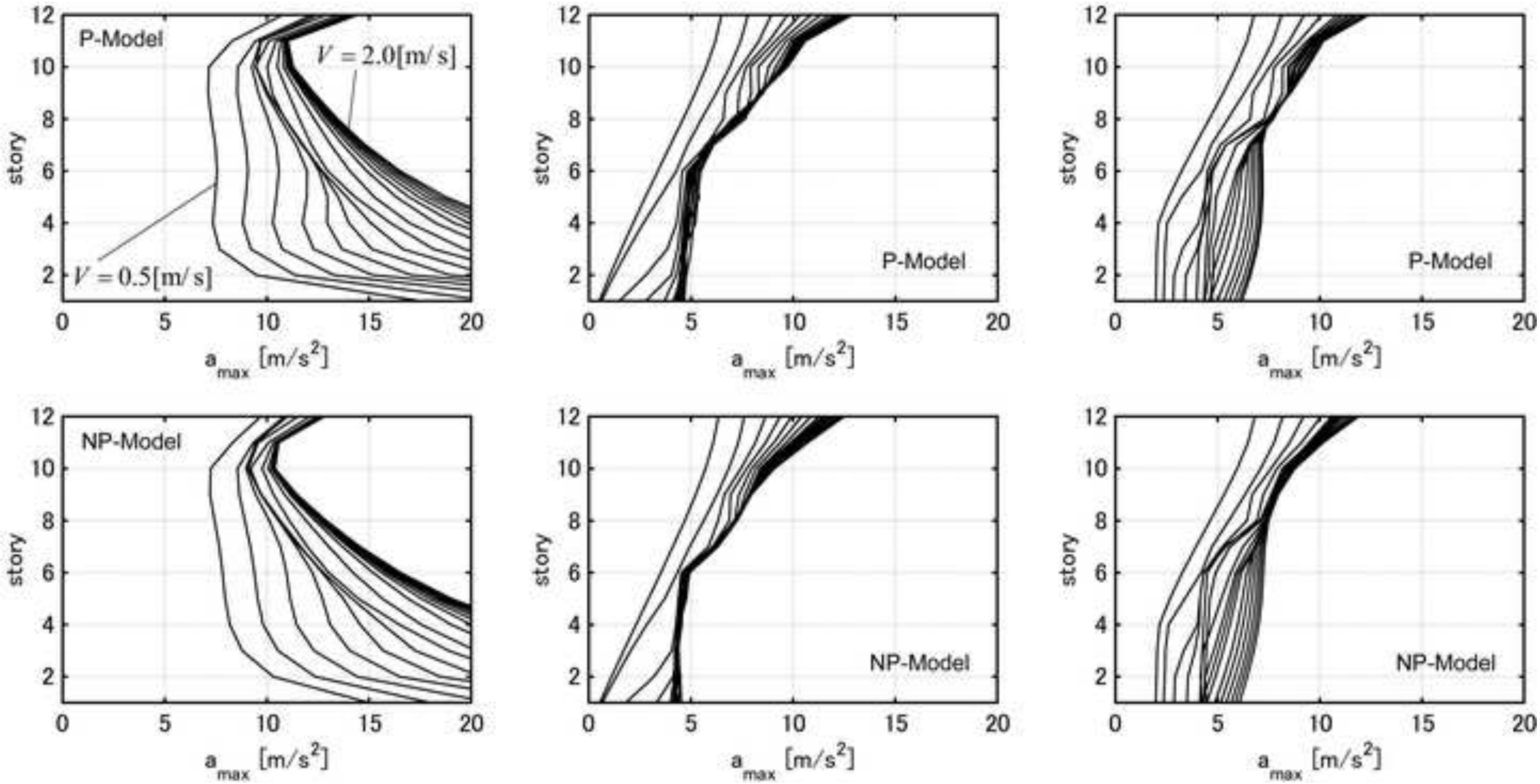
P-Model
$V = 2.0$[m/s]
$V = 0.5$[m/s]
NP-Model
story
a_{max} [m/s²]
12
10
8
6
4
2
0
5
10
15
20

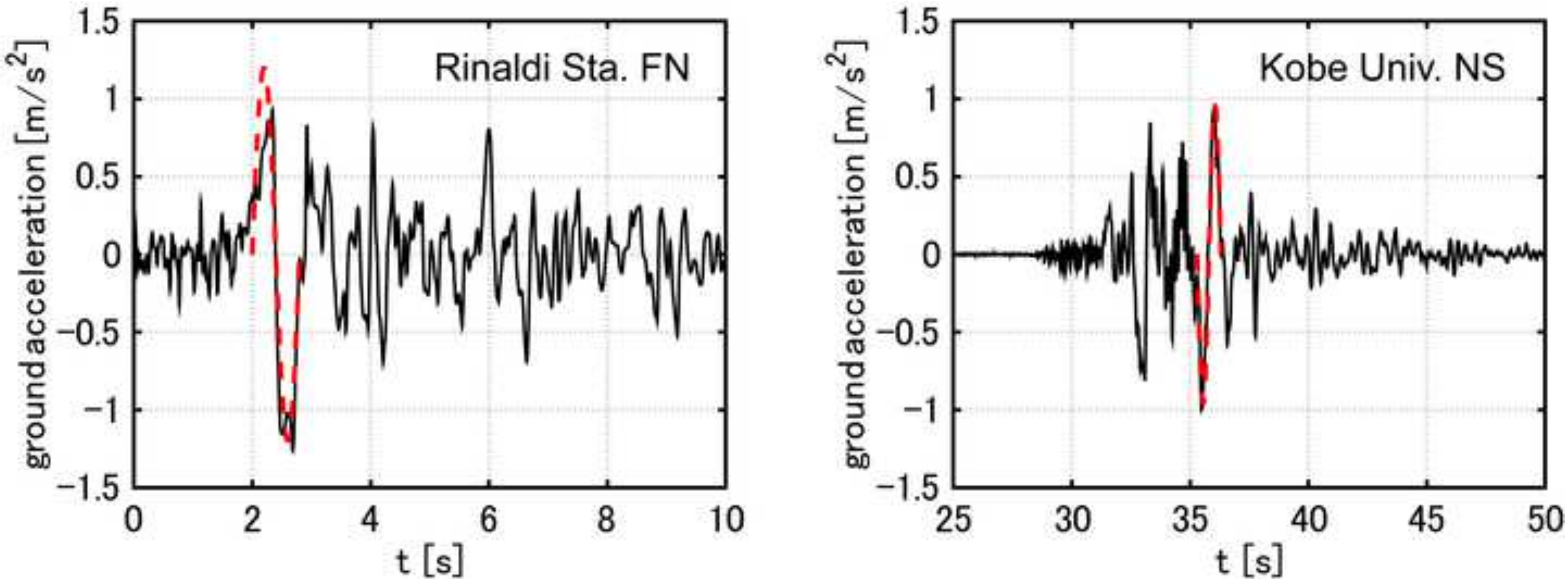
1.5
1
0.5
0
−0.5
−1
−1.5
ground acceleration [m/s2]
Rinaldi Sta. FN
0
2
4
6
8
10
t [s]
Kobe Univ. NS
25
30
35
40
45
50

Click here to access/download;Figure;Fig17.tif

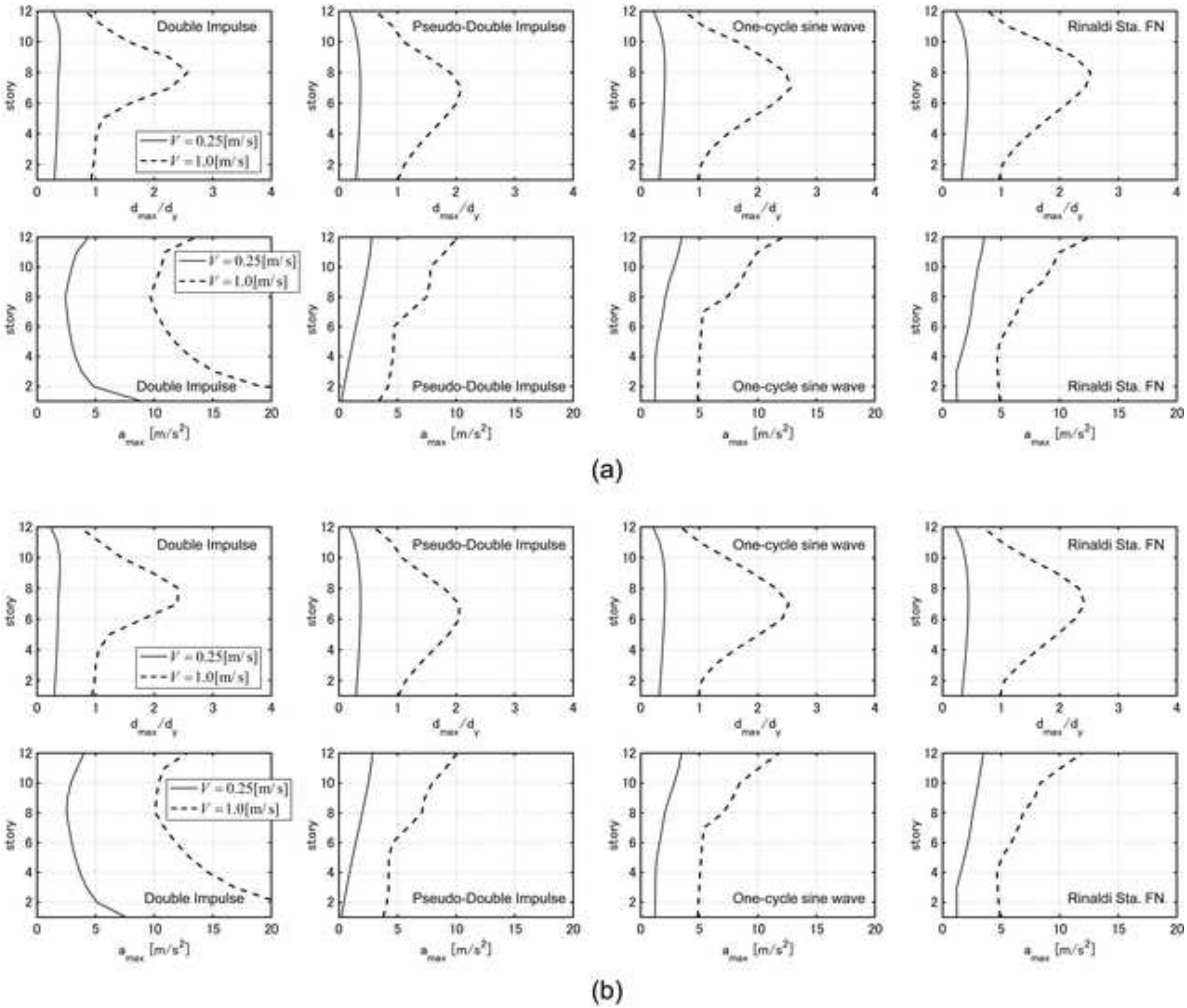

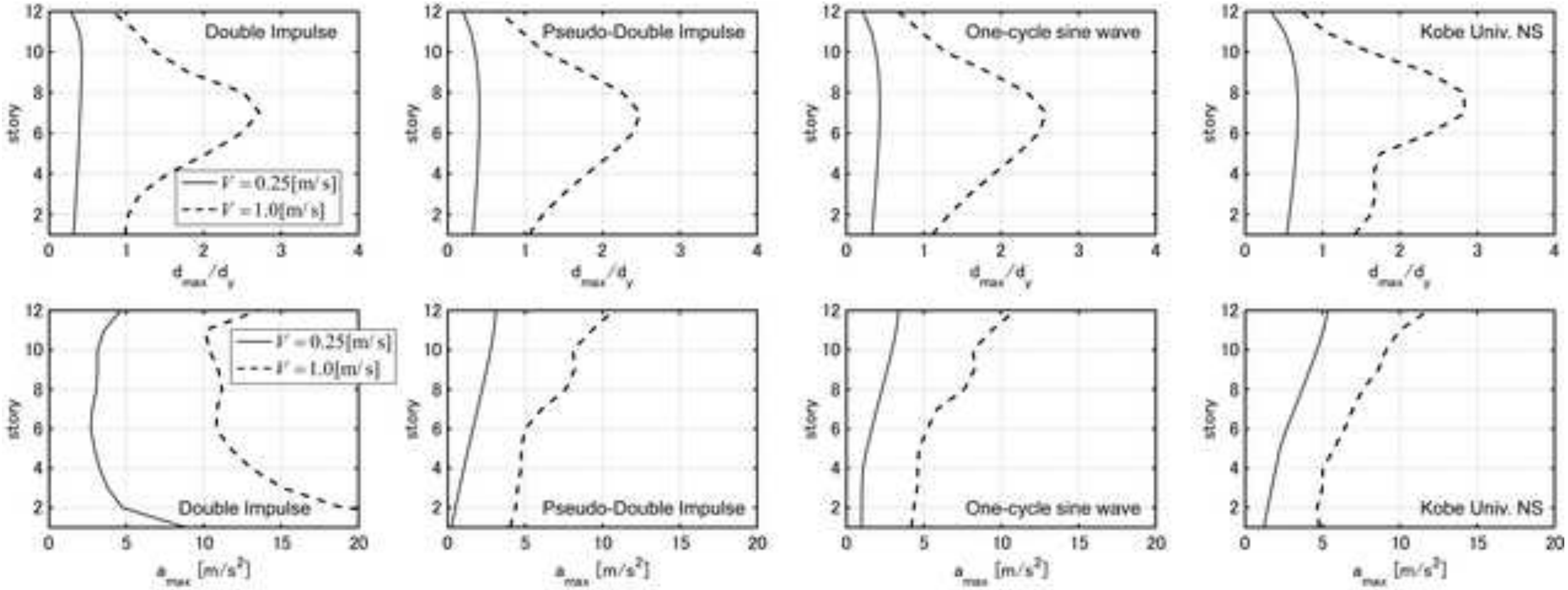
Double Impulse
Pseudo-Double Impulse
One-cycle sine wave
Kobe Univ. NS
V = 0.25[m/s]
V = 1.0[m/s]
story
d_{max}/d_y
a_{max} [m/s^2]

(a)

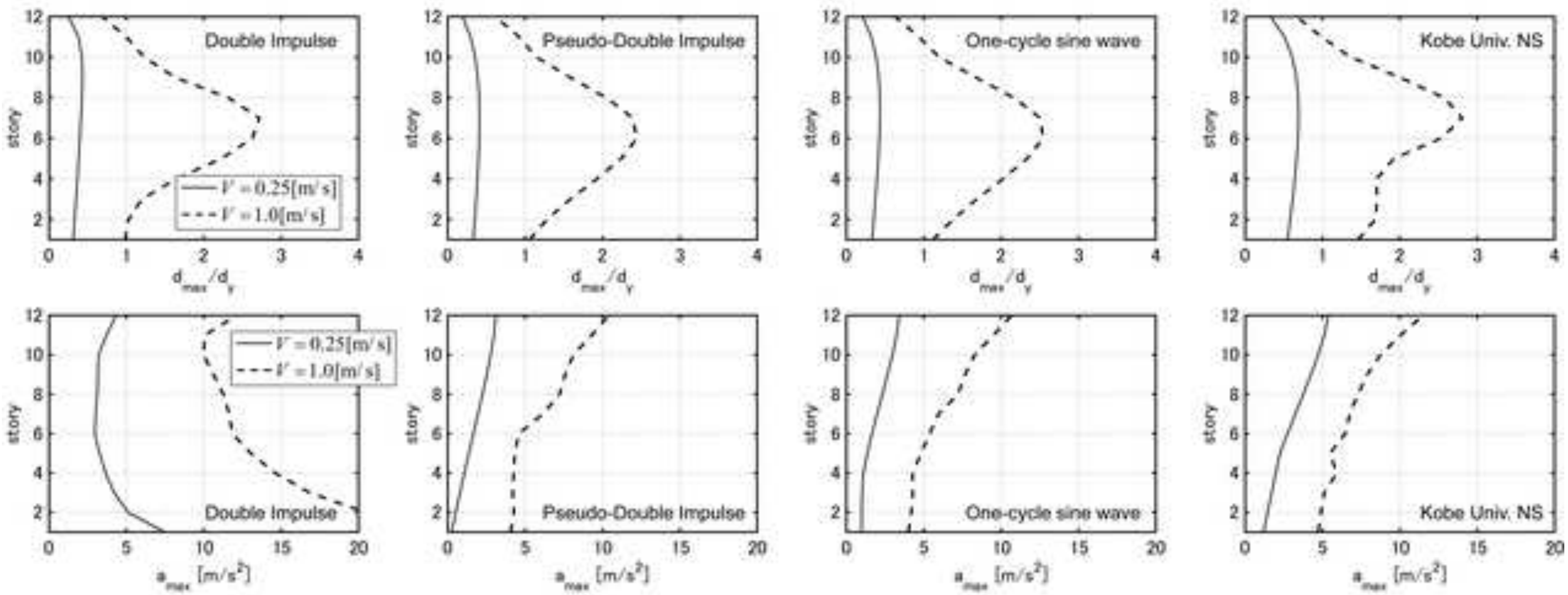
Double Impulse
Pseudo-Double Impulse
One-cycle sine wave
Kobe Univ. NS
V = 0.25[m/s]
V = 1.0[m/s]
story
d_{max}/d_y
a_{max} [m/s^2]

(b)

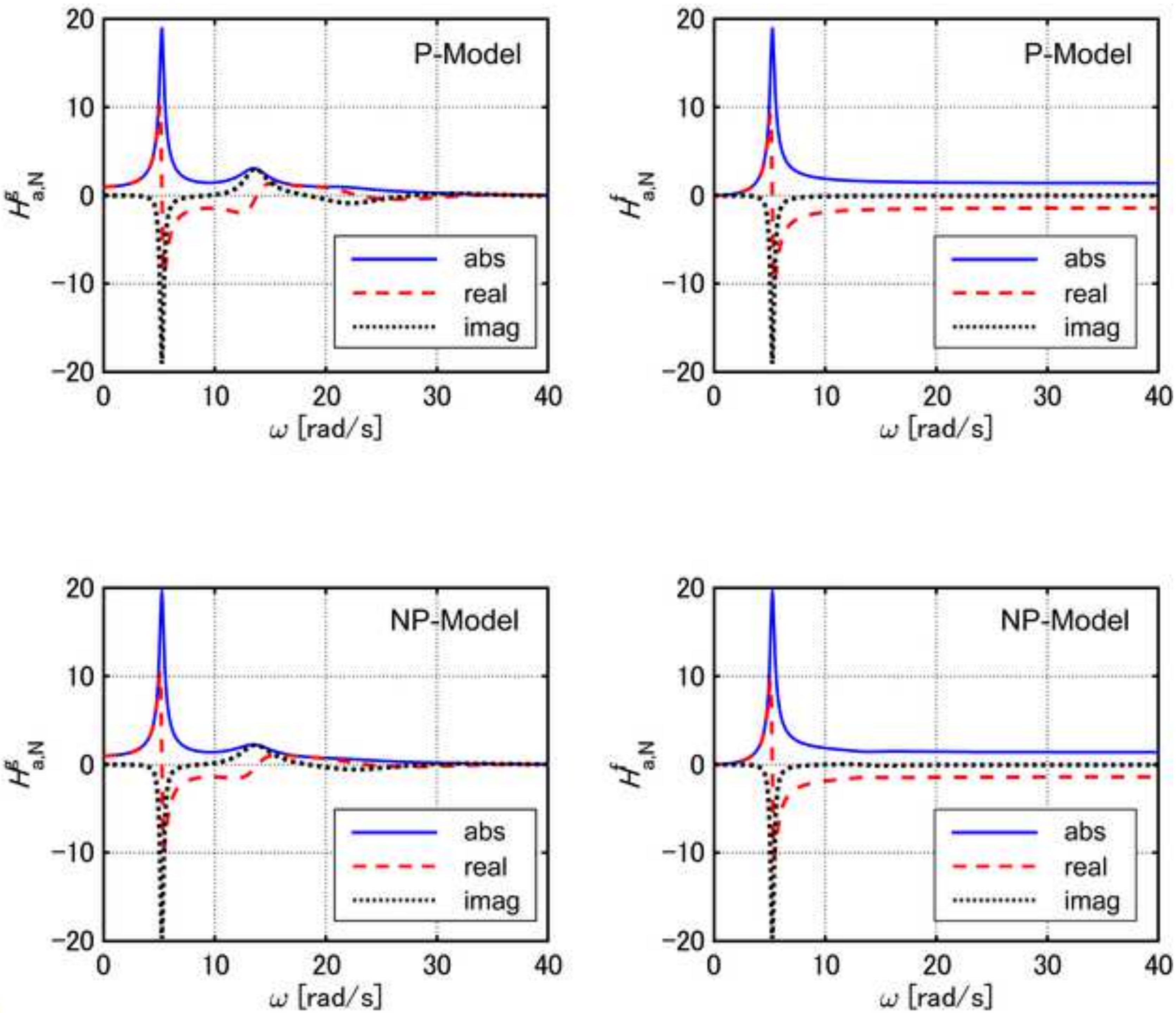
P-Model
abs
real
imag
$H^{\beta}_{a,N}$
ω [rad/s]
P-Model
abs
real
imag
$H^{f}_{a,N}$
ω [rad/s]
NP-Model
abs
real
imag
$H^{\beta}_{a,N}$
ω [rad/s]
NP-Model
abs
real
imag
$H^{f}_{a,N}$
ω [rad/s]

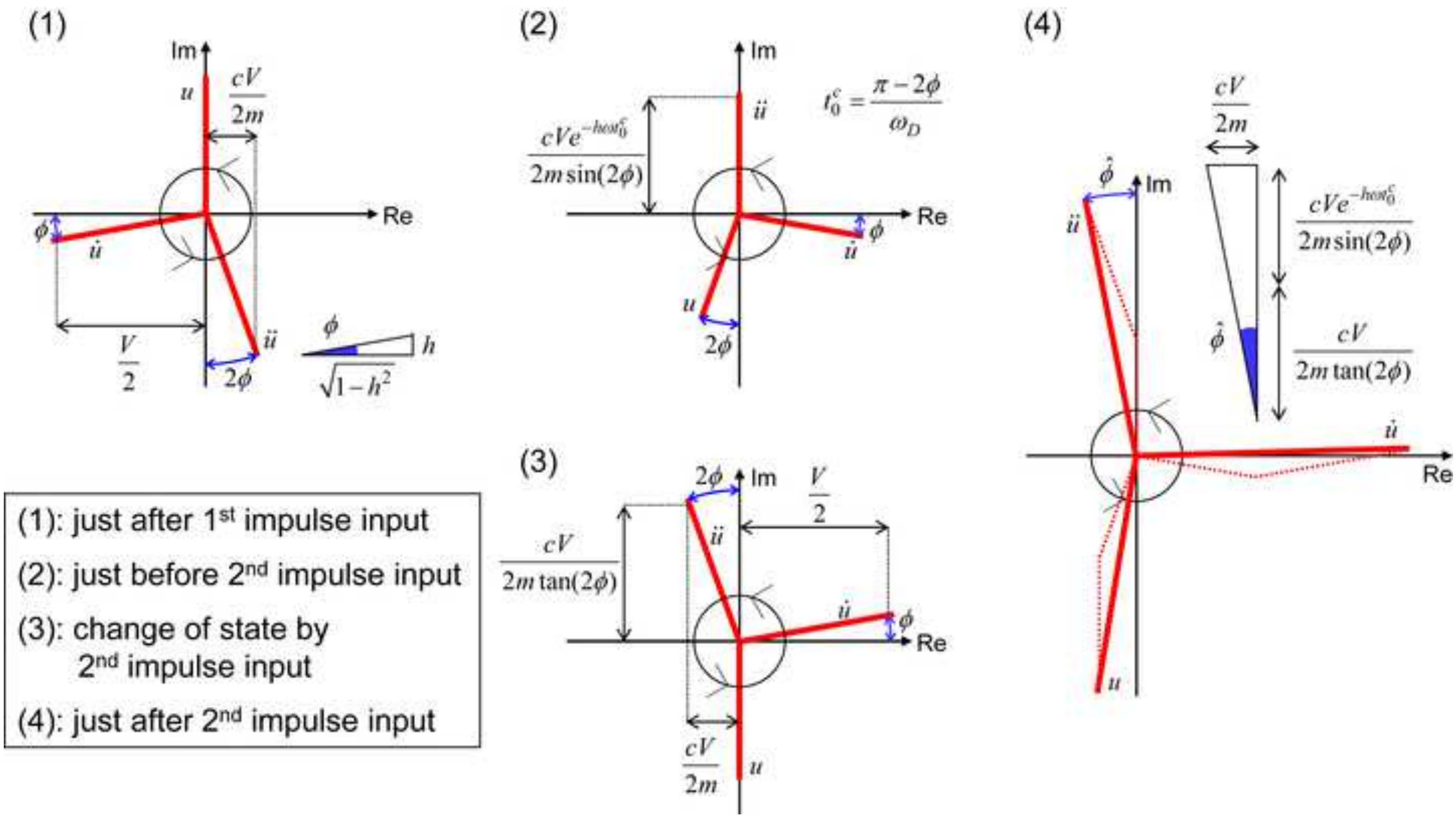
(1)
Im
Re
u
$\frac{cV}{2m}$
ϕ
$\dot{u}$
$\ddot{u}$
$\frac{V}{2}$
2ϕ
h
$\sqrt{1-h^2}$
(2)
$\frac{cVe^{-h\omega t_0^c}}{2m\sin(2\phi)}$
$t_0^c = \frac{\pi - 2\phi}{\omega_D}$
(3)
$\frac{cV}{2m\tan(2\phi)}$
(4)
$\hat{\phi}$
(1): just after 1st impulse input
(2): just before 2nd impulse input
(3): change of state by 2nd impulse input
(4): just after 2nd impulse input